UNIVERSITY OF TWENTE.

BIOS Lab on a Chip group

Detection of chloride ion concentration based on chronopotentiometric sensor-actuator system

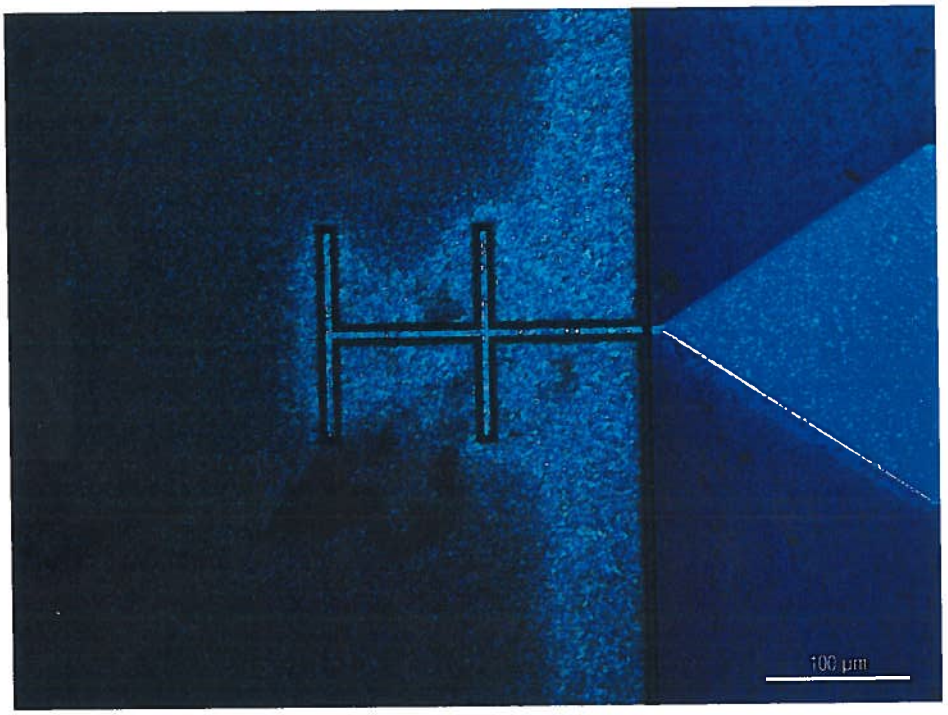

D.B. de Graaf BSc

Master's thesis

August 14, 2013

Examination committee:
prof. dr. ir. A. van den Berg
dr. ir. W. Olthuis
dr. J. Seddon
Y. Abbas MSc

Chair of BIOS Lab-on-a-Chip group
Faculty of Electrical Engineering, Mathematics and Computer Science

Report number: 2013-8

Preface

In the process of obtaining a Master's degree in the field of Electrical Engineering, the last step is to carry out a research project. This work is the result of my final research project and with this report, my education at the University of Twente comes to an end.

I would like to thank a number of people who helped me out with my project and made me enjoy my stay in the BIOS Lab-on-a-Chip group. First of all, I would like to thank Yawar Abbas MSc for being my direct supervisor during the project. I really enjoyed the discussions we had about virtually everything and electrochemistry in particular as they resulted in new insights for me. I also thank Dr. Ir. Wouter Olthuis who, once again, decided to supervise one of my projects. By asking the right questions at the right time and forcing me to keep track of my progress through biweekly meetings, the project was quite successful. Besides that, the door seemed always open if any questions came up. Thirdly I would like to thank Prof. Dr. Ir. Albert van den Berg for letting me stay in the group and taking part in my examination committee. I am grateful to Dr. James Seddon who, although he was not sure what was being asked from him initially, immediately agreed to take part in the examination committee. I am also thankful to Ing. Johan Bomer, who's knowledge of materials and microfabrication techniques made it possible to materialize the theory and who fabricated the chips for me. Without his help, no experiments could have been performed.

The student lab was filled with nice people during my stay and I would like to thank my fellow students for the great time we had together. Especially Luuk, Mathijs and Jan-Yme were both fun to hang around with and very helpful in discussions. Also the PhD students of BIOS are a great asset. From interesting conversations to practical help, they were always there when needed.

Due to sickness in my immediate family, the last few weeks of this project were quite hectic. I had great support during this time from family and friends. Without this support, which came in many different forms, I would not have been able to finish this work in a timely manner. I want to mention my father, Hans, especially in this context as he kept on supporting and pushing me to continue working on the project, even though mine and his mind were not always set to this.

Enschede, August 2013

Preface

Abstract

Chloride ions within reinforced concrete can increase the deterioration of the steel reinforcement. In order to measure this chloride concentration, a measurement system is needed which can detect this chloride ion concentration for prolonged times. Chronopotentiometry is a technique which does not need a long term stable reference electrode and is therefor very suitable for prolonged ion concentration measurements.

With chronopotentiometry, a current pulse is applied to an electrode while the potential of this electrode is observed. In the case of an oxidation reaction, the concentration of the reduced species is lowered due to the ongoing current pulse. At the start of the experiment, a large amount of ions are present near the electrode and the potential will only slowly rise. As the experiment progresses, the concentration drops to zero and a second redox active species will start supplying the electron needed to sustain the applied current. This results in an inflection point in the so-called chronopotentiogram, the plot of the observed electrode potential versus time. The time between the start of the current pulse and this inflection point is called transition time, which is ion concentration dependent and described by the Sand equation.

As the used electrode might be fouled by reaction products, this project focuses on a chronopotentiometric approach with a separated sensing electrode (sensor) and actuating electrode (actuator). A constant current is applied to the actuator while the resulting concentration change is observed through the sensor, which is placed close to the actuator.

To test the separated sensor-actuator approach, a number of test chips were designed, in which the size of the sensor and the distance between sensor and actuator were varied. Using these chips, experiments were done in which the Cl^- ion concentration and applied current density were varied. Also the influence of pH on the measurements were investigated.

The performed experiments show that the sensor senses the local concentration changes resulting from the current applied to the actuator. A linear relation between the Cl^- ion concentration and the square root of the transition time was observed, just as was predicted by the Sand equation.

The calibration curves for the different chips showed that both a larger sensor and a larger distance between sensor and actuator resulted in a larger time delay between the transition time detected at the actuator and the detection time detected at the sensor. The transition time varied with current density as predicted by the Sand equation. For pH>11, proper transition time measurements were no longer possible.

Nomenclature

Abbreviations

AE	Actuating electrode, actuator
BIOS	Lab-on-a-chip chair of the University of Twente
CE	Counter electrode
RE	Reference electrode
SE	Sensing electrode, sensor
UT	University of Twente

Chemicals

AgCl	Silver chloride
BHF	Buffered hydrogen fluoride
Cl^-	Chloride
$FeCl_3$	Iron(III) chloride, ferric chloride
KCl	Potassium chloride
KNO_3	Potassium nitrate
KOH	Potassium hydroxide
OH^-	Hydroxide

Symbols & constants

τ	Transition time [s]
C_i	Concentration of species i [mol/m^3]
d	Distance between sensing and actuating electrodes [m]
D_i	Diffusion coefficient of species i [m^2/s]
E	Electrode potential [V]
F	Faraday's constant (=96 485 sA/mol)
J_i	Flux of species i (net mass-transfer rate) [mol/sm^2]
$k_{i,j}$	Selectivity coefficient with i the primary and j the interfering ion
R	Gas constant (=8.3145 J/Kmol)
T	Absolute temperature [K]
t	Time [s]
w	Line width of the sensing electrode [m]

Contents

1 Introduction

inleiding

1.1 Background

Corrosion of the steel reinforcement in reinforced concrete can weaken the structure over time and decrease the durability of such concrete structures significantly. The steel is normally protected by a thin oxide film, which is formed spontaneously due to the high alkalinity of the concrete. However, this protective film can be damaged by chloride ions; above a certain critical chloride ion concentration, the layer may be locally destroyed and the steel is depassivated [1, 2].

To detect the chloride ion concentration in concrete, a measurement system is needed. Potentiometry is commonly used to determine chloride concentrations, but most this technique needs a stable (liquid junction) reference electrode. Such electrodes are relatively fragile and often need regular recalibration, making long term applications embedded in concrete less feasible [3].

With chronopotentiometry, an electrochemical technique based on potentiometry, the potential of an electrode is measured while a current pulse is applied. Due to ions present in the solution, the resulting chronopotentiogram will show an inflection point when the concentration of a specific ion reaches zero at the surface of the electrode and another ion will start carrying the current. The point in time at which this inflection occurs can be used to determine the concentration of the ion. Since the point in time of the inflection point in the chronopotentiogram is used and not the measured potential itself, the reference electrode has less strict requirements [4].

However, during the experiment, reaction products might precipitate on the electrode, making the surface of the electrode change which will influence the measurement results. To overcome this problem, the functions performed during chronopotentiometry can be divided over two electrodes, i.e. one electrode will carry the current and make sure that a constant amount of ion conversions is done while the potential is measured at a second (non-current carrying) electrode. This work investigates the function of such a separated sensor-actuator system.

1.2 Project description

The aim of this master thesis project is to give a proof of concept for the separated sensor-actuator system for measuring chloride concentration. The general topic of the assignment is therefor:

Detection of the chloride ion concentration based on a chronopotentiometric sensor-actuator system

This research topic is divided over a number of research questions:

- What parameters influence the functioning of the sensor-actuator system?
- What is the effect of the current density on the measurements?

- Does the pH-level of the solution influence the chloride concentration measurements?
- Are the experimental results in accordance with theory?

1.3 Outline of this report

This report continues with the theoretical analysis in Chapter 2. Based on the theory, a chip design is presented in Chapter 3. The measurement setup and protocol can be found in Chapter 4. Chapter 5 shows the experimental results of this work and compares it with the theoretical background. Conclusions drawn from this report as well as an outlook to extend this research and recommendations for similar projects are given in Chapter 6.

Five appendices are added to the end of this report. Appendix A gives the derivation of a part of the theory. In Appendix B, the MATLAB script used to perform digital simulation is presented. The designed mask is given in Appendix C and the used cleanroom process is presented in the process document in Appendix D. Finally, the MATLAB scripts used to do some data analysis can be found in Appendix E.

2 | Theory

In this chapter, the theory used in this research project is introduced. In Section 2.1, the used electrochemical techniques are introduced. Section 2.2 expands this basic theory to fit the system introduced in this work. This chapter ends with a short summary of the introduced theory in Section 2.3.

2.1 Electrochemical measurement methods

2.1.1 Potentiometry

With potentiometry, the potential of a working electrode is measured with respect to a reference electrode at almost zero current (schematically visualized in Figure 2.1). Since the potential of the reference electrode is constant (by definition, because of its standardized design), the measured potential at the working electrode is a function of the concentration of electroactive species in the electrolyte.

If the working electrode is driven to more negative potentials, electrons in the electrode gain more energy and an electron flow from the electrode to the solution (reduction current) occurs. Likewise, a more positive potential lowers the energy of the electrons, resulting in an electron flow from the solution to the electrode, i.e. an oxidation current. Logically, there exists an electrode potential with which no net electron transfer takes place [5, 6].

Assuming a true equilibrium state at electrode potential E with respect to the reference electrode, the equilibrium of Equation 2.1 exists:

$$\mathrm{ox} + n \cdot \mathrm{e} \rightleftarrows \mathrm{red} \tag{2.1}$$

with n the number of electrons involved in the redox reaction. If the working electrode would be forced to a potential E', an amount of work would be used to oxidize n mol of red into ox (given that $E' > E$) equal to [6, p. 234]:

$$n\left(E' - E\right)F \qquad \left[\mathrm{J/mol}\right] \tag{2.2}$$

where F is Faraday's constant. The ratio between the concentrations of red and ox ions can be derived from Boltzmann statistics [6, p. 234]:

$$\frac{C_{ox}}{C_{red}} = e^{\frac{-\alpha}{RT}} \tag{2.3}$$

which is the fraction of species having an extra energy of at least α. R is the gas constant, T the absolute temperature [K] and C_i is the concentration of species i in $\mathrm{mol/dm^3}$. The extra energy α is obtained by the increased electrode potential.

By substituting the amount of work (Equation 2.2), resulting from the increased potential, into Equation 2.3 we can define the ratio of red and ox concentrations that results from the increased potential [6, p. 234]:

$$\frac{C_{ox}}{C_{red}} = e^{\frac{-n(E'-E)F}{RT}} \tag{2.4}$$

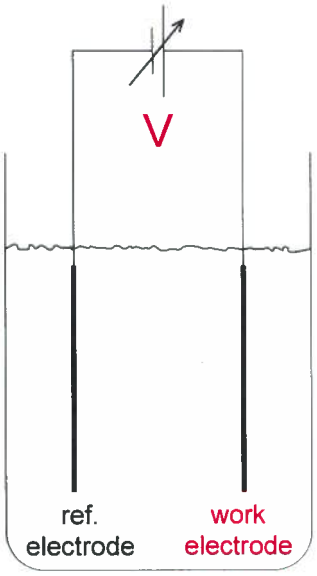

Figure 2.1: Schematic representation of an electrochemical cell for potentiometry. Image taken from Olthuis [5, p. 80].

This relation is also valid for the case in which only the assumed potential E exists ($E' = 0$):

$$\frac{C_{ox}}{C_{red}} = e^{\frac{nEF}{RT}} \tag{2.5}$$

which can be rearranged into:

$$E = \frac{RT}{nF} \ln\left(\frac{C_{ox}}{C_{red}}\right) \quad [\mathrm{V}] \tag{2.6}$$

The assumed concentration dependent electrode potential E has to be added to the standard potential E^0, which is the electrode potential of a specific redox couple under standard conditions (unity concentrations of 1 mol/dm^3 at 101.3 kPa and $T = 298$ K). The resulting identity is known as the Nernst Law [4–6]:

$$E_{Nernst} = E^0 + \frac{RT}{nF} \ln\left(\frac{C_{ox}}{C_{red}}\right) \quad [\mathrm{V}] \tag{2.7}$$

Potentiometry is a well established method for determining a species' concentration. Selectivity for a particular species can be increased by the use of a ion-specific membrane covering the electrode. A big advantage of potentiometry is the relatively simple instrumentation required: a high ohmic voltmeter is all that is needed for a measurement. Since potentiometry is a zero current technique, the power requirements for a potentiometric system are generally low [7].

However, there are some downsides to potentiometry. The biggest drawback is the necessity of a well defined reference electrode, since the measured potential is directly dependent on this reference. For proper measurements, the system needs to be recalibrated regularly. Also, the Nerst equation (Equation 2.7) predicts potential changes in the order of millivolts for concentration changes of a factor of two, making an accurate reference and careful temperature control (to decrease the variation of T) even more important. Established reference electrodes depend on liquid junctions with an electrolyte of constant composition. In applications where the reference electrode is hard to reach, it might be difficult, if not impossible, to change the electrolyte to prevent potential drifts. In such cases, pseudo-references are sometimes used: electrodes whose potential is based on a background ion which has a constant concentration for the duration of the measurement. Nevertheless,

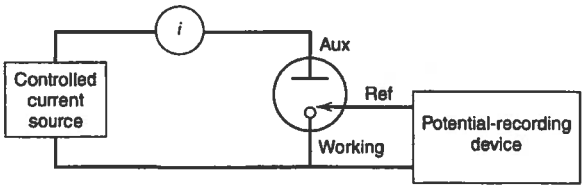

Figure 2.2: Simplified diagram of a setup for chronopotentiometric measurements. Image taken from Bard and Faulkner [4, p. 305]

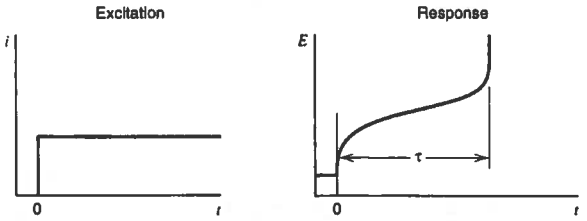

Figure 2.3: Theoretical response for constant-current potentiometry. Image taken from Bard and Faulkner [4, p. 307]

such stable background ions are not always available, rendering the pseudo-reference electrode useless. [7].

When careful (re)calibration is not an option, such as in hard to reach systems which do measurements for prolonged periods of time, potentiometry cannot be used. However, a derived form of potentiometry in which the exact potential is not of importance, but only a change in potential is observed, can still be used: chronopotentiometry.

2.1.2 Chronopotentiometry

When potentiometry is performed while running a controlled current through the working electrode, the resulting potential is a function of time. The current is applied trough a working electrode and an auxiliary, counter electrode, since reference electrodes are based on potentiometry and require (almost) zero current to get a reliable signal. The resulting setup is depicted in Figure 2.2 [4].

In the case where a constant current runs through the working electrode, an electrochemical species is oxidized or reduced at a constant rate. The remainder of this paragraph will describe an oxidation reaction ($\mathrm{red} \rightarrow \mathrm{ox} + n \cdot \mathrm{e}$), but the same theory could be inverted for the case of a reduction reaction. The potential of the electrode will be characteristic for the redox couple and varies with time as the concentration of red and ox at the electrode surface changes (following the Nernst equation, 2.7). After some time, the concentration of red will drop to zero at the electrode surface. At this point, the flux of species toward the electrode is no longer sufficient to supply all of the electrons needed to sustain the forced current. The potential of the electrode will quickly shift to more positive values at this point. Zero concentration would result in an infinitely positive potential (as visible in Figure 2.3), which is never reached in real situations. Instead, a second redox process will occur, providing the electrons not supplied by the initial redox couple. The point in time at which the concentration of red at the electrode reaches (almost) zero and thus the potential shift occurs, is called transition time (τ) [4, 8].

General theory

To get an analytical expression for the transition time, Fick's laws of diffusion are essential. Starting with Fick's first law [4, 6]:

$$-J_{red}(x,t) = D_{red}\frac{\delta C_{red}(x,t)}{\delta x} \qquad [\text{mol/sm}^2] \tag{2.8}$$

where $J_{red}(x,t)$ is the flow of red molecules that pass a location at time t at a distance of x from the electrode, D_{red} the diffusion coefficient for red and $C_{red}(x,t)$ the concentration of red. Fick's second law deals with the change of concentration per time [4, 6]:

$$\frac{\delta C_{red}(x,t)}{\delta t} = D_{red}\left(\frac{\delta^2 C_{red}(x,t)}{\delta x^2}\right) \qquad [\text{mol/sm}^3] \tag{2.9}$$

Assuming a planar working electrode at $x = 0$, an unstirred solution (making it possible to neglect convection), high concentration of background electrolyte (to neglect migration) and only red species initially present with concentration C^*_{red}, a number of boundary conditions can be formulated. The first is the constant concentration throughout the solution at $t = 0$:

$$C_{red}(x,0) = C^*_{red} \tag{2.10}$$

The red concentration far away from the electrode is assumed to be undisturbed by the oxidation process:

$$\lim_{x\to\infty} C_{red}(x,t) = C^*_{red} \tag{2.11}$$

Since the current running through the electrode $i(t)$ is the controlled parameter, it should be known. With the current known, the flux at the surface of the electrode is given by [4, p. 308]

$$D_{red}\left[\frac{\delta C_{red}(x,t)}{\delta x}\right]_{x=0} = \frac{i(t)}{nFA} \qquad [\text{mol/sm}^2] \tag{2.12}$$

where A is the surface area of the electrode.

Using the boundary conditions of Equation 2.10 and 2.11, Equation 2.9 is transformed using the Laplace method (refer to Appendix A for the full transformation) to [4, p. 308]:

$$\bar{C}_{red}(x,s) = \frac{C^*_{red}}{s} - \frac{\bar{i}(s)}{\sqrt{\frac{s}{D_{red}}}nFAD_{red}}e^{-\sqrt{\frac{s}{D_{red}}}x} \tag{2.13}$$

where $\bar{f}(s)$ denotes the Laplace transformed version of a function $f(t)$.

Constant-current chronopotentiometry

If the current is kept constant, i.e. $i(t) = I$, then $\bar{i}(s) = I/s$. Equation 2.13 now becomes:

$$\bar{C}_{red}(x,s) = \frac{C^*_{red}}{s} - \frac{I}{\sqrt{\frac{s^3}{D_{red}}}nFAD_{red}}e^{-\sqrt{\frac{s}{D_{red}}}x} \tag{2.14}$$

The inverse Laplace transform (using [4, p. 771]) of Equation 2.14 renders an expression for the concentration of red-ions [4, p. 309]

$$C_{red}(x,t) = C^*_{red} - \frac{I}{nFAD_{red}}\left[2\sqrt{\frac{D_{red}t}{\pi}}\,e^{-\frac{x^2}{4D_{red}t}} - x\,\text{erfc}\left(\frac{x}{2\sqrt{D_{red}t}}\right)\right] \qquad [\text{mol/m}^3] \tag{2.15}$$

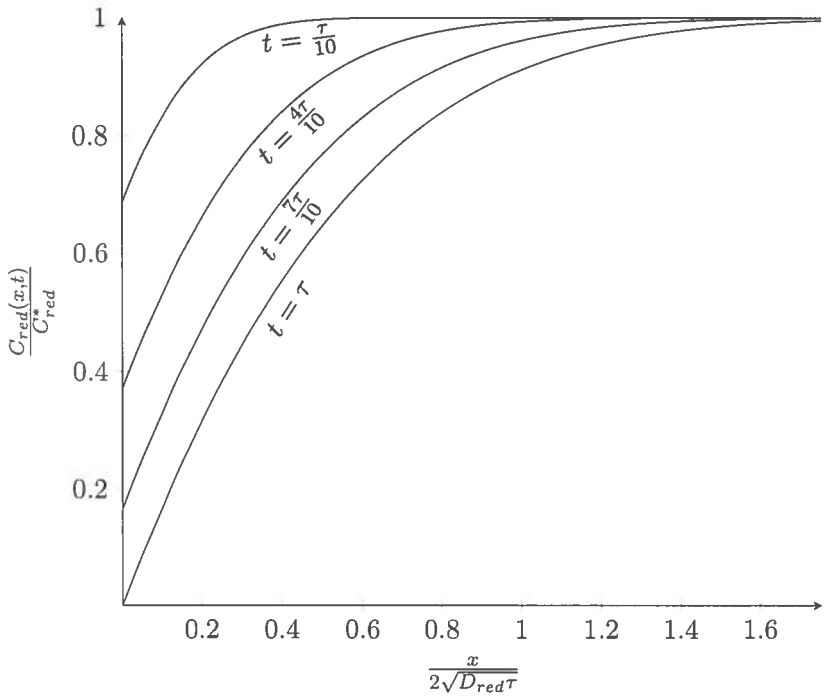

Figure 2.4: Normalized concentration profile for various values of t, as indicated in graph.

Typical (normalized) concentration profiles at various times are shown in Figure 2.4.

The concentration at the electrode can be found by setting $x = 0$ in Equation 2.15:

$$C_{red}(0,t) = C^*_{red} - \frac{2I}{nFA}\sqrt{\frac{t}{D_{red}\pi}} \qquad [\text{mol/m}^3] \tag{2.16}$$

As noted before, the concentration at the electrode will drop to zero after some time. This transition time can be found by setting $C_{red}(0,t) = 0$ in Equation 2.16 and rearranging. The result is known as the Sand equation [4, p. 310]

$$\tau = \frac{D_{red}\pi}{4}\left(\frac{nFAC^*_{red}}{I}\right)^2 \qquad [\text{s}] \tag{2.17}$$

The expression for the concentration (Equation 2.15) can be combined with the Nernst equation (Equation 2.7):

$$E(x,t) = E^0 + \frac{RT}{nF}\ln\left(\frac{C_{ox}(x,t)}{C_{red}(x,t)}\right) \qquad [\text{V}] \tag{2.18}$$

Based on Equation 2.18 and assuming that the reaction product ox in $\text{red} \rightarrow \text{ox} + n \cdot \text{e}$ is solid, in which case C_{ox} can be taken as 1, the graph of Figure 2.5 can be drawn. In this graph, the potential is given at the electrode ($x = 0$) and a small distance from the electrode ($x = 5\mu\text{m}$). The potential at the electrode however, is purely theoretical and will never be measured at the working electrode, as the Nernst equation assumes zero current. When a current is flowing, additional phenomena, such as resistive losses in the solution, will influence the measured potential.

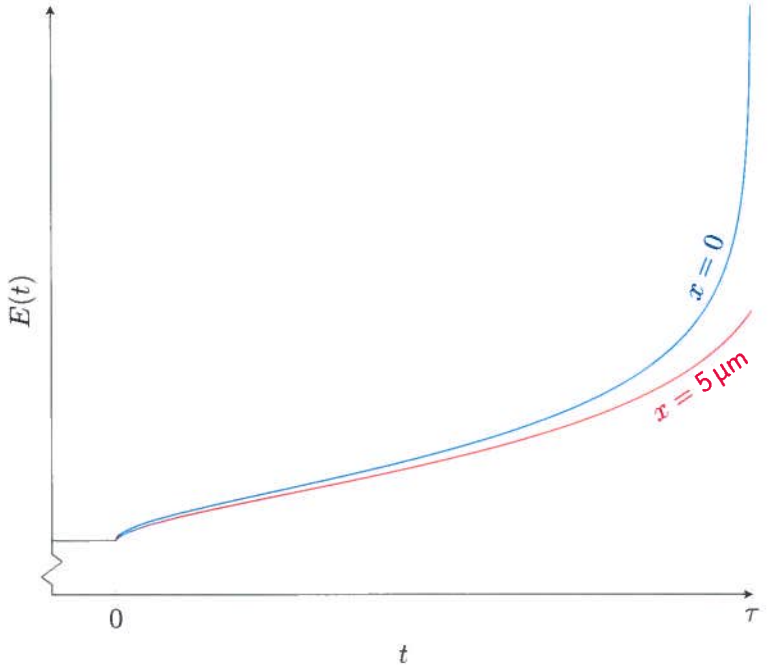

Figure 2.5: Theoretical chronopotentiogram for a nernstian process with concentration $C_{ox} = 1$ at distance x from a planar electrode. A constant current is applied at $t > 0$.

Although the (theoretical) transition time can be determined easily by a sharp rise in the measured potential, as can be seen in Figure 2.5, there should be enough information at an earlier point in time to determine the transition time. Equation 2.17 can be rearranged into:

$$\frac{2I}{nFA\sqrt{D_{red}\pi}} = \frac{C^*_{red}}{\sqrt{\tau}} \tag{2.19}$$

Combining Equation 2.16 with Equation 2.19 results in:

$$C_{red}(0,t) = C^*_{red}\left(1 - \sqrt{\frac{t}{\tau}}\right) \tag{2.20}$$

When this relation is inserted into Equation 2.18 and again assuming a solid reaction product ox, the result has the form of Equation 2.21:

$$E(x,t) = E^0 + \frac{RT}{nF}\ln\left(\frac{1}{C^*_{red}}\right)\ln\left(\frac{1}{1-\sqrt{\frac{t}{\tau}}}\right) \tag{2.21}$$

The second derivative of this expression shows a root at $\tau/4$. Since τ is directly related to the initial ion concentration, this means that if this inflection point can be detected in the chronopotentiogram, the concentration can be determined four times faster. This prevents fouling of the electrode as the amount of precipitation (in case of a solid reaction product) can be limited. However, in noisy signals, the inflection point is often not clearly visible as it is a very subtle change, as can be seen in Figure 2.6.

2.1.3 Chronopotentiometric response of Ag/AgCl

The theory presented before can be applied to this specific project, which focuses on determining the chloride (Cl^-) concentration. In this case, a silver electrode with a layer of silver chloride (AgCl)

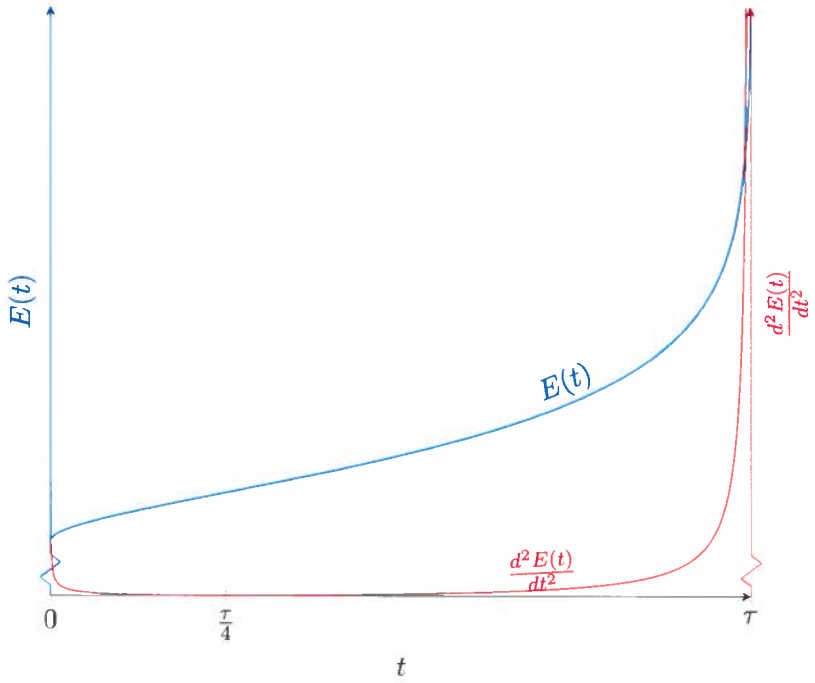

Figure 2.6: Theoretical chronopotentiogram and its second derivative. The second derivative shows a root at $\tau/4$.

is used as working electrode. Such a Ag/AgCl electrode is commonly used as (pseudo-)reference electrode and therefor widely studied [9, 10]. A diffusion coefficient D_{Cl^-} of 2.03 m/s^2 is reported [13, p. 143]

Chronopotentiometry in this case is performed by forcing a current into the Ag/AgCl working electrode. This results in the following oxidation reaction:

$$\mathrm{Ag[s] + Cl^-[l] \longrightarrow AgCl[s] + e^-} \tag{2.22}$$

A drawback of this system is the consumption of Ag during the measurements, which will eventually lead to an electrode which is no longer sensitive to chloride. Also, the reaction product, AgCl, will form a layer on top of the electrode surface, which will eventually lower the reaction rate, as it takes time for Ag particles to diffuse through the AgCl layer toward the surface.

After the Cl^- concentration at the electrode has gone to zero, a second oxidation reaction will occur. The most likely candidate for this second reaction is the reaction with water, forming :

$$\mathrm{2\,Ag[s] + O-[aq]->Ag_2O[s] + e^-} \tag{2.23}$$

This reaction forms silver oxide, which affects the functioning of the device as it will cover the AgCl layer, making it harder for Ag particle to reach the electrode surface.

The Ag/AgCl electrode shows a higher selectivity to Cl^- than to other interfering ions which might be present [3]. In concrete, the most notable interfering ions are hydroxide ions (OH^-), which come from the hydration of $Ca(OH)_2$, NaOH and KOH [11]. Interference occurs if the ratio of Cl^- to OH^- ions is in the range of or lower than the so-called selectivity coefficient, a coefficient indicating how sensitive an electrode is to an ion compared to another ion [3, 11]. The selectivity coefficient for OH^- ions in aqueous solutions as the interferent for Cl^- at an Ag/AgCl electrode, k_{Cl^-,OH^-}, is reported as 2.4×10^{-2} [12].

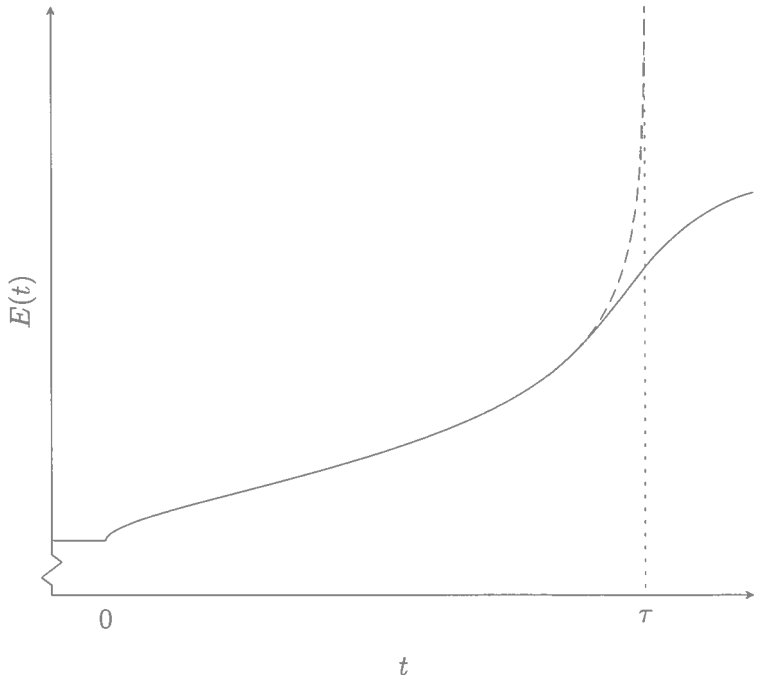

Figure 2.7: Sketch of the response for constant-current potentiometry with multiple redox couples present. The dashed line gives the theoretical response for one redox couple as seen in Figure 2.5.

2.2 Separation of sensing and actuation

The transition time is observed by a potential shift of the electrode, which happens at the moment that the concentration of the species, which is the most favorable to exchange its electrons, reaches zero and the second most favorable reaction will start to take place. The resulting chronopotentiometric curve will show a "S" shape such as the one sketched in Figure 2.7. The inflection point in the curve can be taken as the point determining the transition time, but it can only be observed after the second reaction has started, as only a (theoretical) system with one single redox active species being present would give a chronopotentiogram similar to Figure 2.5. If the reaction product precipitates on the electrode, the electrode surface changes, which possibly has an influence on the measurements.

In the case of this project, the initial redox couple taking care of the electron flow is the Ag/AgCl reaction as given in Equation 2.22. The second reaction occurring is most likely the reaction with oxygen, as given in Equation 2.23. After the transition time, the electrode shows a mixed potential as a result of both redox reactions occurring concurrently.

By separating the actuation and sensing function of the electrode into two separate electrodes, some problems can be overcome. Earlier work by the BIOS chair has resulted in integrated sensor/actuator devices for coulometric purposes [14, 15].

The sensing electrode (SE) or sensor can be a purely potentiometric device, where no current is flowing and therefor no (electrochemical) fouling can occur. Also the potential drop occuring at electrodes which carry a current will not be visible.

Another electrode, which will be called actuating electrode (AE) or actuator will be used to carry the current to deplete the concentration of the species of interest at its surface. The exact potential of this electrode is of less importance, since the amount of current represents the amount of species converted [4, p. 4].

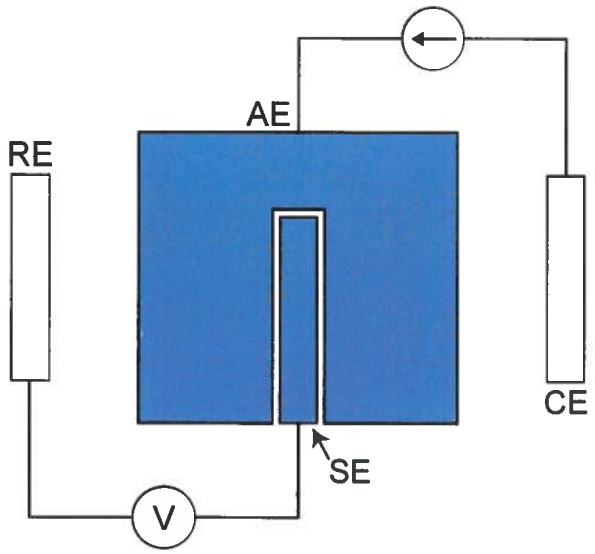

Figure 2.8: Schematic representation of the electrode setup with separated sensor and actuator. RE=reference electrode, CE=counter electrode, SE=sensing electrode, AE=actuation electrode

Figure 2.8 gives a schematic representation of the separated sensor and actuator setup. As can be seen in this figure, a current is drawn through the actuator and a potential is measured at the sensor (versus a reference electrode (RE)). Figure 2.5 shows that in a system with one redox couple present, the transition time is not clearly visible if the concentration at 5 µm perpendicular to the planar actuator is measured using potentiometry. Therefor, the one dimensional model used until this point needs to be expanded. Also note that this setup is basically the electrochemical equivalent of the four point probes measurement technique commonly used in electrical engineering.

2.2.1 Concentration profile after the transition time

As mentioned before, at transition time the flow of species toward the electrode is no longer sufficient to deliver the forced current and the potential will rise until another redox couple can provide the needed amount of electrons. However, ions of the initial redox couple, ($Ag + Cl^- \leftrightarrows AgCl + e^-$ in this case) will still diffuse toward the electrode. Since the potential of the electrode is above the Nernst potential, the ions will oxidize. This means that part of the current is still handled by the initial redox couple. Although the concentration at the electrode will remain zero, the concentration level some distance from the (actuating) electrode is changing due to the ongoing diffusion. To get an idea of the concentration level at the sensing electrode and the resulting observed potential, this diffusion is further investigated.

With regard to the initial redox couple, the circumstances at $t \geq \tau$ are the same as for an amperometric experiment (refer to Figure 2.4 for $t = \tau$), i.e. zero concentration at the electrode, bulk concentration far away from the electrode and a diffusion controlled flux of ions toward the electrode. However, often a homogeneous solution at the start of the amperometric experiment ($t = \tau$ in this case) is assumed, such as for the Cottrell equation, which describes the current flow through an electrode as a result of a suitable potential step [4, pp. 162-163]. Since at $t = \tau$ the concentration is not constant, but follows Equation 2.15, the mathematics are greatly complicated and do not result in usable expressions.

Still, the problem can be approached using digital simulation. As digital simulation needs a discrete model, the solution is divided into a number of finite 'bins'. Figure 2.9 shows an example of such a division. If the size of the bin Δx and the simulated time step Δt are taken small enough

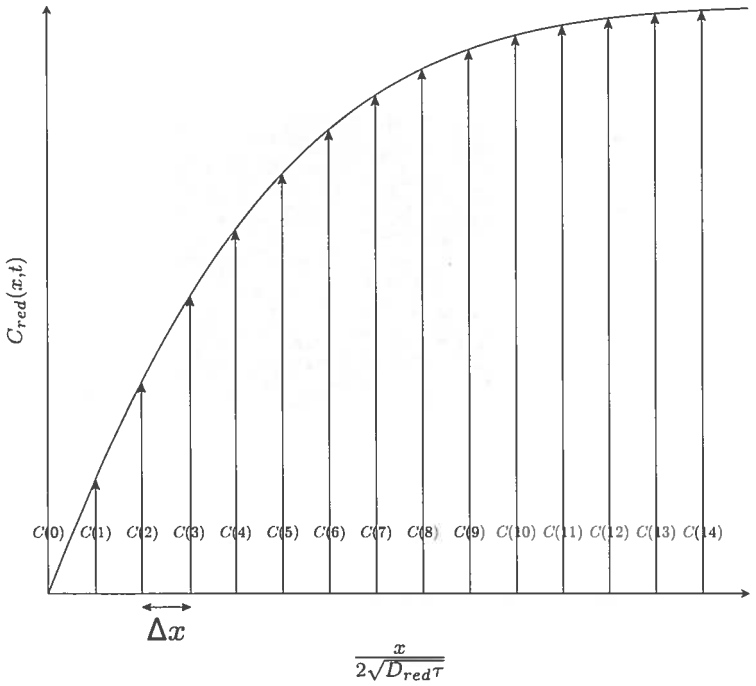

Figure 2.9: Discrete model of the solution

($D\Delta t/\Delta x^2 < 0.5$ [4, p. 791]), it can be assumed that diffusion only occurs between direct neighbors, i.e. in the simulated time step only the concentration difference between adjacent bins determines the concentration level in the next iteration of the simulation. To calculate the concentration levels, the following equation can be used [4, pp. 785-787]:

$$C\left(x,t+\Delta t\right)=C\left(x,t\right)+\frac{D_{red}\Delta t}{\Delta x^2}\left[C\left(x+\Delta x,t\right)-2C\left(x,t\right)+C\left(x-\Delta x,t\right)\right] \tag{2.24}$$

in which Δx is the size of the bin and Δt is the amount of time simulated per iteration.

Each iteration, the concentration at the electrode (bin $C(0)$ in Figure 2.9) is set to zero, to simulate the reaction at the electrode (Equation 2.22). The initial concentration levels follow from Equation 2.15 with $t = \tau$. Appendix B shows the full MATLAB script used to do this simulation and another script used to obtain specific data from the simulation output.

Using the simulation data, Figure 2.10 can be expanded to include the profile after the transition time, as shown in Figure 2.10. As noted before, until the transition time, the current supplied by the initial redox couple is constant, which can be seen by the constant angle the curves make with the y-axis ($[\delta C(x,t)/\delta x]_{x=0}$) for $0 < t \leq \tau$. For $t > \tau$, this constant current cannot longer be sustained, which is visualized in Figure 2.10 by the change in $[\delta C(x,t)/\delta x]_{x=0}$.

Figure 2.11 presents the normalized concentration over time for different distances perpendicular to the electrode. For $x > 0$, the concentration change per time ($\delta C(x,t)/\delta t$) is a lot lower for $t > \tau$. This is due to the fact that the difference between the bulk concentration (C^*) and the concentration at the electrode ($[C(0,t)]_{t>\tau}$) is no longer changing, however the slope is declining as a result of the diffusion profile extending further into the solution, thus increasing Δx.

The change in $\delta C(x,t)/\delta t$ would be visible in a chronopotentiogram as inclination point if an electrode would be placed at the given distance x perpendicular to the actuating (i.e. current carrying), planar electrode at $x = 0$. Theoretically, this chronopotentiogram would look like Figure 2.12.

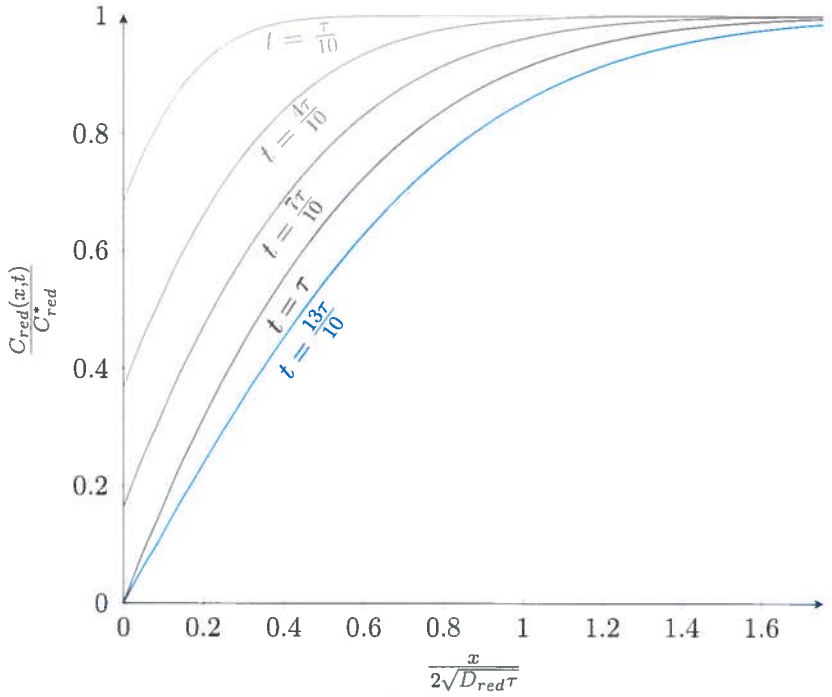

Figure 2.10: Normalized concentration profile for various values of t, as indicated in graph. A constant current is applied at $t > 0$.

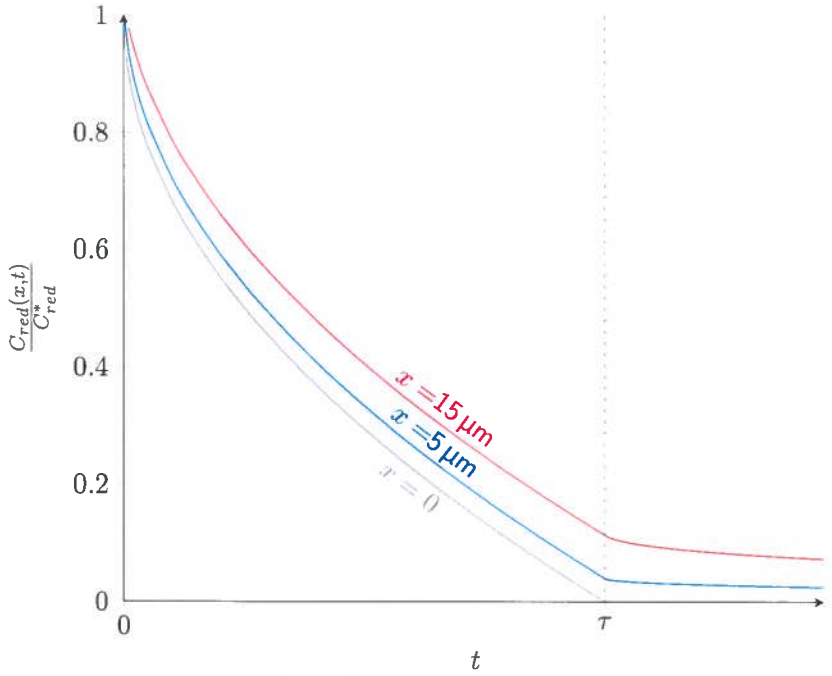

Figure 2.11: Normalized concentration over time at $x = 0$, $x = 5\,\mu m$ and $x = 15\,\mu m$. A constant current is applied at $t > 0$.

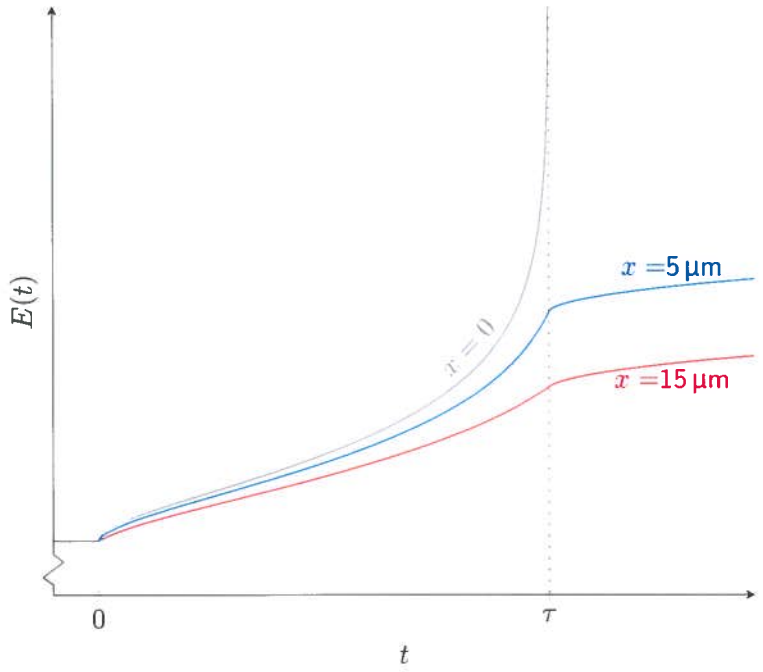

Figure 2.12: Theoretical chronopotentiogram for a nernstian process with concentration $C_{ox} = 1$ at distance $x = 5\,\mu m$ and $x = 15\,\mu m$ from a planar electrode, assuming only the initial redox couple determines the potential. For reference, the theoretical chronopotentiogram for $x = 0$ is given. A constant current is applied at $t > 0$.

It is assumed in this chronopotentiogram that only the initial redox couple influences the potential at the electrode at distance x from the actuating electrode at $x = 0$, in this project that would mean that only the Cl^- ion concentration determines this potential and no mixed potential is observed. As can be seen in the chronopotentiogram, in this case an inflection point occurs at $t = \tau$ in the chronopotentiometric measurement at distance $x > 0$ from the electrode. This inflection point becomes less pronounced for larger x.

2.3 Summary

In this chapter, a number of electrochemical techniques were introduced. First, potentiometry was explained. With this zero current technique, a potential is observed at a working electrode with respect to a reference electrode. This potential is ion concentration dependent and follows the Nernst equation (Equation 2.7). The second introduced technique was chronopotentiometry. In this technique, a current pulse through the working electrode depletes all ions at the surface of the electrode. When the potential of the working electrode is observed, the moment in time at which the ion concentration at the electrode drops to zero is visible as an inflection point in the so-called chronopotentiogram. The time between the start of the current pulse and this inflection point is called transition time. This transition time is concentration dependent and described by the Sand equation (Equation 2.17). The specific case of Cl^- ions and the Ag/AgCl electrode was further investigated, as this research project is focused on the measurement of Cl^- ion concentration.

The remainder of this chapter introduced a separated sensor-actuator approach, in which a current pulse runs through an actuating electrode while the potential change is observed at a second, sensing electrode placed near the actuating electrode. A one dimensional model was used to get an idea of the expected sensor behavior.

3 | Design

To verify the functioning of the separated sensor-actuator approach, a number of chips are designed. Section 3.1 introduces the design choices that were made and the resulting chip characteristics. In Section 3.2, the cleanroom fabrication process is introduced.

3.1 Design choices

Based on the theory of Chapter 2, a number of design considerations can be determined. First of all, the distance between sensor and actuator can be varied. A small distance between the two ensures that the concentration of species at the surface of the sensor is strongly influenced by the concentration change at the actuator's surface. However, this distance is limited by the fabrication technology available to this project.

reference technology limit

Secondly, the size of the sensing electrode can be varied. A smaller sensor has less influence on the shape of the diffusion profile of the Cl^- ion concentration at the actuator. Another benefit of a small sensor is that it takes less time for the diffusion profile to travel over the sensor or, in other words, there is less variation of the concentration level over the sensor surface. A drawback of a small sensor is that the contact lines toward the sensor can form an area similar in size or even larger than the area which was intended to be the sensing part.

Thirdly, the size of the actuator is of importance for the design. A large actuator will ensure that the diffusion profile is extending into the solution, perpendicular to the electrode surface. On the other hand, a smaller actuator requires lower current levels to reach a specific current density level than would be needed with a larger electrode.

The fourth and last design consideration is the shape of the sensor. The benefit of a interdigitated design is that a sensor with a fixed surface area and line width is confined in a smaller area than a straight line with the same width and surface area, decreasing the chance of measuring mixed potentials, i.e. measuring an average potential as a result of different concentration levels at different locations of the electrode. If the sensor gets too wide, the influence of the actuator decreases as it takes more time for a certain concentration profile to fully cover the sensor surface.

In this project, an interdigitated design was chosen with a double T shape (see Figure 3.1. The smallest design (Design 1), was based on technology constraints, i.e. a line width w of 5 µm and a distance d between sensor and actuator of 5 µm. Since the sensor has contact lines running toward it, a part of the silver surface will not have an actuator in the direct vicinity. To compensate for this, the area of the sensor was taken 100 times larger than the sensor area with no actuator area nearby (more than d between the edge of the sensor and the edge of the actuator), which results in a total exposed sensor area of 2.5×10^{-9} m^2. The actuator was designed to be a lot larger than the sensor, with an area over 2000 times larger (5.4×10^{-6} m^2) than the area of the sensor. To prevent contact lines from acting as additional electrode area, parts of the chip are insulated with a polyimide, which is shown in blue in Figure 3.1.

The second design, Design 2, has $w = 20\,\mu m$ with the sensor surface area scaled accordingly (times 4^2), which results in a total sensor area of $4.0 \times 10^{-8}\,m^2$. The actuator area is now over 200 times larger ($8.5 \times 10^{-6}\,m^2$) than the sensor area. The distance between sensor and actuator was kept constant at 5 µm.

The third design, Design 3, has an even larger thickness of w =50 µm, which increases the sensor surface area to $2.5 \times 10^{-7}\,m^2$. The actuator area has been increased to $1.6 \times 10^{-5}\,m^2$. The distance between sensor and actuator in this design is 5 µm.

The forth and last design (Design 4) uses the same sensor parameters as Design 1 ($w = 5\,\mu m$), but d between sensor and actuator has been increased to 15 µm. The actuator has an area of $5.6 \times 10^{-6}\,m^2$.

3.2 Chip fabrication

This section gives a short overview of the chip fabrication process. The full process document by Ing. Johan Bomer can be found in Appendix D.

The chips are fabricated using boroflot glass wafers as substrate. The electrodes consist of a layered structure or titanium, platinum and silver. Titanium is used as a adhesion promotor between the metal structures and the substrate. Platinum is used as a barrier to prevent diffusion between the titanium and the silver layer. The metals are sputtered into a recess etched into the substrate by a buffered hydrogen fluoride (BHF) solution, in such a way that the top of the metal structure will be level with the surface of the substrate.

Conventional lithography combined with a lift off process is used to pattern the metal layers. Parts of the chip are passivated by a polyimide (Durimide 7505), a polymer consisting of imide monomers, to cover the contact lines. Titanium is again used as an adhesion promotor, this time to improve the adhesion of the polyimide layer to the electrode, with again a platinium diffusion barrier in between. The full structure is shown in Figure 3.2. The used polyimide is photosensitive and can therefore be patterned directly after spincoating the polymer on the surface. Metal areas not covered by the polyimide layer are then partly etched back to get to the silver surface.

3.3 Summary

The design process resulted in four chip designs consisting of a double T shape sensing electrode, surrounded by a larger actuating electrode. The distance between the sensor and actuator (d) and the line width of the sensor (w) are varied between the chip designs. The electrodes on the chip consist of titanium, platinum and silver and specific regions of the metal structures are passivated by a polyimide cover.

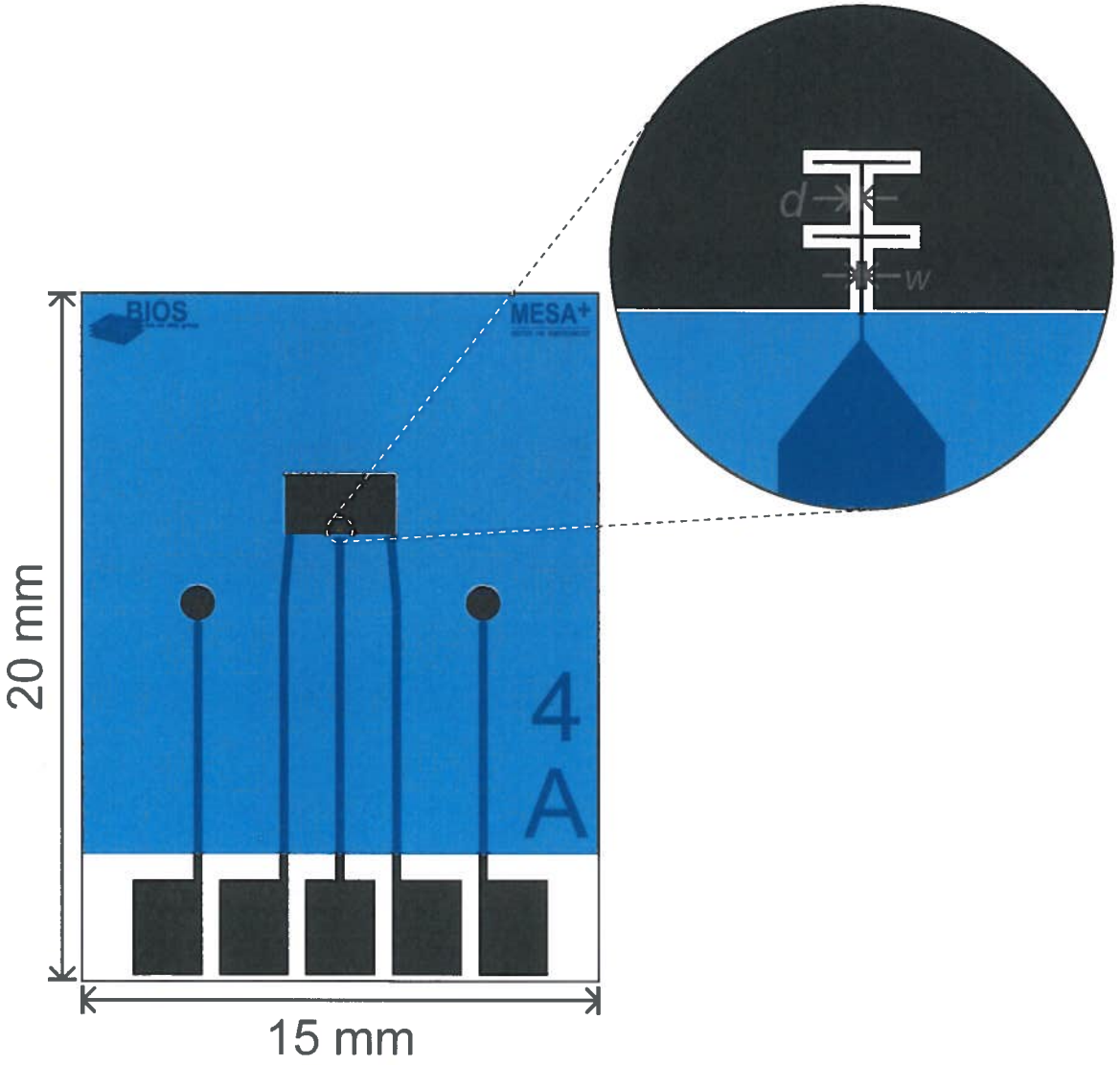

Figure 3.1: Example of the design of the chips (image shows Design 4) with d the distance between sensor and actuator and w the line width of the sensor electrode. The inset shows a close-up look of the design. Black structures are the silver electrodes, contact wires and contact pads, blue colored parts will are insulated areas covered by a polyimide.

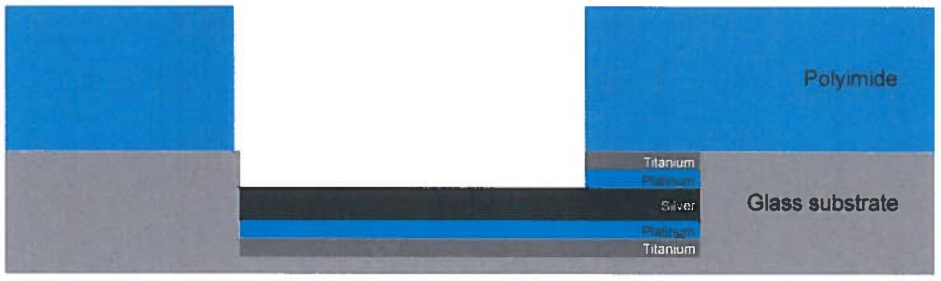

Figure 3.2: Cross-section of the structure of the chip design. Shown thicknesses are not drawn to scale.

4 Method & materials

Experimental work has to be performed to verify the theoretical working of the sensor-actuator system. Section 4.1 presents the used chemicals. Instruments and software needed for this project is given in Section 4.2. The setup used to perform the experiments with is introduced in Section 4.3. Using this setup a number of experiments will be performed, which are described in Section 4.4.

4.1 Chemicals

Potassium chloride (KCl, BioXtra, $\geq$ 99.0%), potassium hydroxide (KOH, $\geq$ 90% pure reagent grade), potassium nitrate (KNO_3, ReagentPlus®, $\geq$99.0%) and hexahydrated iron(III) chloride ($FeCl_3 \cdot 6\,H_2O$, 98-102%) were obtained from Sigma-Aldrich, the Netherlands. Solutions were prepared using DI-water, deionized by a Millipore Milli-Q system.

4.2 Instrumentation and software

The experiments were conducted using a BioLogic SP-300 potentiostat controlled with BioLogic EC-Lab software (versions V10.31 and V10.32). Sonication was performed by a VWR ultrasonic cleaner. MathWorks MATLAB R2012a (7.14.0.739) was used for data analysis and manipulation. Optical inspections were done using a Leica DM6000M optical microscope with Leica Application Suite 4.2.0 software.

4.3 Experimental setup

The measurement setup consists of a custom-made teflon experimental cell, in which one of the designed chips can be placed, as shown in Figure 4.1. The custom-made cell consists of the parts shown in Figure 4.2. The chip is electrically connected to the potentiostat through spring contacts. Besides the chip, two additional electrodes are placed inside the cell: a commercial Ag/AgCl reference electrode and a platinum counter electrode.

Two measurement channels of the potentiostat are used in 'CE to ground'-mode and connected as visible in Figure 4.3. In this setup, the reference and counter electrodes are connected to both channels.

4.4 Measurement procedure

4.4.1 Chip preparation

The chips are stored in oxygen free cabinets, in which a constant flow of nitrogen prevents oxide formation. Before experiments can start, the chip is sonicated for five minutes in DI-water to remove glass particles on the surface that are the result of the wafer dicing. No chemical cleaning is

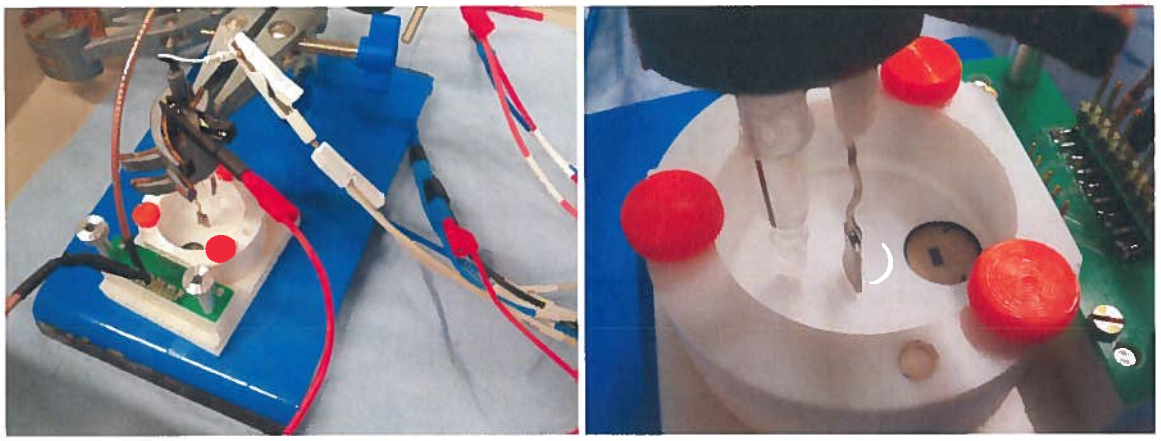

A B

Figure 4.1: Photos of the setup. (A) an overview of the chip holder with attached wires. (B) a close-up picture of the chip holder. Inside the chip holder the electrodes are visible. From left to right: a Ag/AgCl reference electrode, a platinum counter electrode and the designed chip, inside the circular hole in the chip holder.

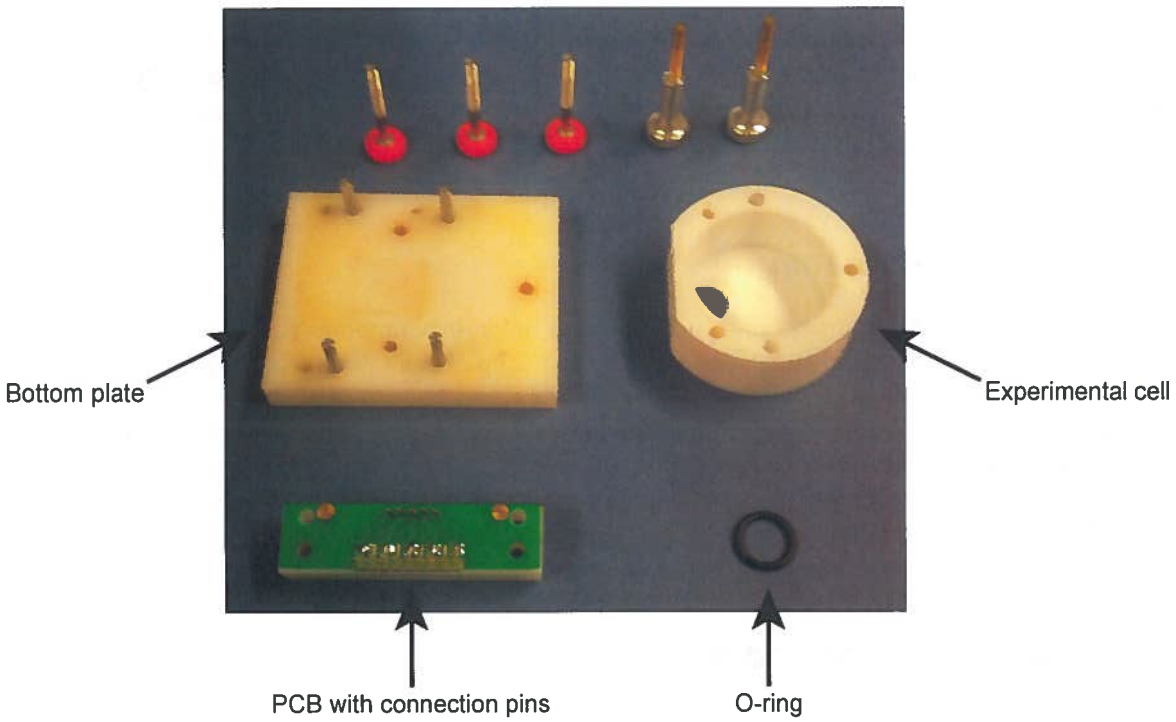

Figure 4.2: Photos of the parts of the custom-made electrochemical cell.

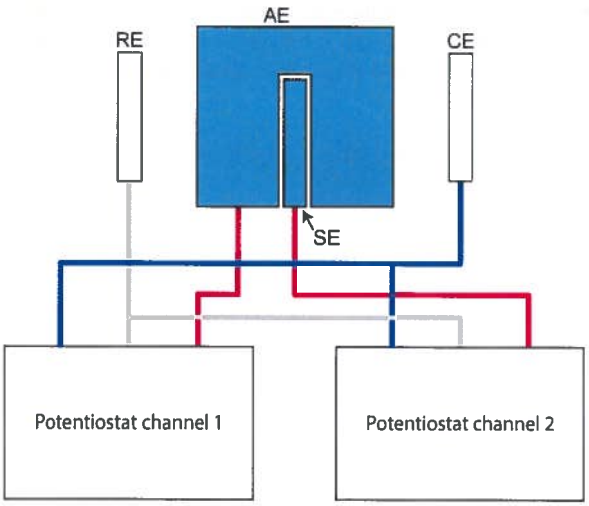

Figure 4.3: Schematic of the electrical connections to the electrochemical cell. RE=Ag/AgCl reference electrode, CE=Pt counter electrode, SE=on-chip sensing electrode, AE=on-chip actuator electrode

performed as the chips were stored clean since they came out of the cleanroom and the cleaning process might affect the polyimide cover layer.

The silver electrodes need to have a silver chloride layer on top to get a Ag/AgCl electrode. Electroless deposition is used to deposit AgCl as this gives the most uniform layer, although the process is less controlled as would be the case with electrodeposition. Iron(III) chloride ($FeCl_3$), also known as ferric chloride is used in this process, resulting in the following reaction taking place:

$$Ag[s] + FeCl_3[l] \longrightarrow AgCl[s] + FeCl_2[l] \tag{4.1}$$

A chip is secured in the experimental cell before 2 mL of 0.1 M ferric chloride solution is added. After 30 s, the solution is poured out of the cell and extensively rinsed with DI-water. The chip is dried using an air blow gun. The chips are visually inspected to verify that the electrodes are covered by a gray layer of AgCl over the Ag electrodes. Color differences in this gray layer indicate a non-uniform layer and are a reason to reject the chip for use in experiments.

4.4.2 Chronopotentiometric measurement

After the depostion of AgCl over the Ag electrodes, the chip is ready to perform the experiments with. The electrochemical cell is filled with 5 mL solution which, depending on the experiment and unless otherwise noted, initially consists of 1 mM KCl and 0.5 M KNO_3. In these experiments, low chloride concentration levels (mM-range) are chosen as higher current levels are required to deplete higher concentrations locally in the same time frame, which would degrade the actuator electrode much faster. In this work, a current density of 10 A/m^2 is used, unless otherwise noted. This current density in combination with concentrations in the order of several mM KCl results in expected transition time (according to the Sand equation, Equation 2.17) within 10 s. KNO_3 acts as a background electrolyte to prevent migratory effects and be able to regard this system as being diffusion controlled.

The potentiostat is connected as depicted in Figure 4.3. The first channel (connected to the actuator) is set up as a normal chronopotentiometric experiment, in which a constant current is applied for some time. To prevent the chips from oxidizing after the depletion of Cl^- ions near the electrode, the potential is level limited; i.e. when the chosen potential is reached, the current is set to zero. Oxide formation alters the electrode surface, locally forming Ag_2O which impedes locally the proper function of the Ag/AgCl electrode. As a result, current densities might locally change,

Table 4.1: Volume of solution removed and solution with higher concentration added to increase the total concentration. When the initial concentration is 1 mM, the second column indicates how much volume should be replaced by a solution with concentration 10 mM to get the concentration in column one. The replaced volume is indicted with respect to the previous line.

Concentration [mM]	Replaced volume [mL]
1	-
2	0.556
3	0.625
4	0.714
5	0.833
6	1.000

affecting the diffusion profile and thus the measurement results. The second channel is configured to measure the potential (open cell voltage or OCV). All measurements are performed in a Faraday cage to prevent external noise sources influencing the measurement result.

When the KCl concentration has to be increased, for instance to obtain calibration curves, a portion of the used solution is taken out of the cell and replaced by an equal volume of solution with a KCl concentration of one higher order. Table 4.1 shows the concentration series with required replaced volumes of higher concentration.

4.4.3 Measurement series

To characterize the designed sensor-actuator system, a number of experiments should be performed. The first experiment involves investigating the sensor-actuator system by obtaining a calibration curve. This is done by measuring the response of the sensor for different Cl^- concentration. The series starts at 1 mM and goes in 1 mM steps up to 6 mM (which gives an expected transition time at the actuator under 5 s). As a background electrolyte, 0.5 M KNO_3 is used.

To investigate the influence of sensor line width w and the distance d between sensor and actuator (refer to Figure 3.1) on the system, similar calibration curves are obtained for the different chip designs. Comparing the calibration curves should point out the influence of the two parameters.

To assess the influence of the current density applied to the actuator on the measurement results, a solution with 3 mM KCl and 0.5 M KNO_3 is used. The current density is varied from 3 A/m^2 to 10 A/m^2. According to the Sand equation, the transition time at the actuator should stay under 15 s with these concentration and current densities. A limited transition time is needed to prevent convection having a significant influence on the system.

The influence of pH (hydroxide ions) is investigated using a solution consisting of 1 mM KCl, 1 M KNO_3 and varying amounts of KOH. By varying the KOH concentration, the pH of the solution can be altered. Given the selectivity coefficient of the Ag/AgCl (refer to Subsection 2.1.3), pH-levels of 11, 12 and 13 were chosen. pH 11 corresponds to a OH^- concentration of 1 mM and so the KCl concentration should be dominant in the measurement results. With pH 12 (10 mM OH^-) and 13 (100 mM OH^-), the OH^- concentration is expected to have a larger influence on the measurement results, since (for pH=13) the concentration of OH^- ions times the selectivity coefficient is in the same order as the KCl concentration.

Although this project aims at presenting a proof of concept for separated sensor-actuator chronopotentiometry, the stability of the measurement system over time is assessed. Using a constant KCl concentration of 3 mM and 0.5 M KNO_3, measurements are taken with about an hour in between each other. The sensor is kept in the solution in between measurements.

4.4.4 Data analysis

Obtained measurement results are converted from the EC-Lab software into tab delimited ".MPT" files using the export function of EC-Lab. The number of digits is set to 6 as the 'auto' function of the program generally results in the loss of precision. A number of MATLAB functions have been written to import the MPT-files and extract the transition time from them. These functions can be found in Appendix E.

4.5 Summary

This chapter introduced the used chemicals, intrumentation and software. The measurement setup consists of a custom-made experimental cell in which the chip can be secured. Before the measurements commence, the chips are prepared by sonication and electroless deposition of AgCl. After inspection, the chip can be used for experiments.

In the experiments, a solution consisting of KCl and KNO_3 is used. Calibration curves are obtained by varying the KCl concentration in between measurements. Also the current density is varied. In some cases, the pH is changed by an addition of KOH to check the result of interference by OH^- ions.

5 Results & discussion

The results from the experiments as presented in Chapter 4 are presented in this chapter. First, the result of the cleanroom process is discussed in Section 5.1. General observations done during the experiments are treated in Section 5.2. The first calibration curve is presented in Section 5.3. In Section 5.4, the calibration curve of a chip with a larger sensor is compared with the calibration curve of Section 5.3. Section 5.5 also compares calibration curves, this time between chips with a different distance between the sensing and actuating electrode. The current density applied to the actuator is varied in Section 5.6. The influence of pH on the measurements is discussed in Section 5.7. The stability of the measurement results was not always optimal and this is further investigated in Section 5.8. The chapter ends with a summary of the obtained results.

5.1 Fabrication results

Two wafers (following the mask design of Appendix C) were produced, resulting in six chips of each of the four chip designs. For test purposes, one of the wafers lacked the top platinum layer in between the silver layer and the covering titanium layer (refer to Figure 3.2), resulting in less process steps. While doing the experiments, no differences were observed between chips with and without the second platinum layer. However, some chips with the additional platinum layer seemed less clean when they came out of the clean room.

Some chips showed deformations such as bended etches of the electrodes or not fully etched trenches. Figure 5.1 shows an example of a chip with production faults. Production faults only occurred at some chips with larger line widths ($w = 20\,\mu\text{m}$ and $w = 50\,\mu\text{m}$).

5.2 Observations from the experiments

Chronopotentiograms come in the form of Figure 5.2. Using the first derivative (approximated by the MATLAB script in Listing E.5 of Appendix E as the measured signal is time discrete), the point of inflection is located and the transition times can be extracted. As the chronopotentiogram shows small signal variation due to white noise, the MATLAB script filters the original chronopotentiogram using a running average filter before the derivative is calculated. This filtering might result in a small time shift in the detected transition time.

In some of the measurements, such as the one in Figure 5.2, the derivative of the sensor signal shows a small peak near the inclination point of the actuator response (indicated by a circle in Figure 5.2). This is likely due to a resistive connection through the solution between the two electrodes.

As expected, the actuator signal shows an ohmic drop at the start of the current pulse. The sensor response also shows a small jump in the signal, again likely caused by a resistive path between sensor and actuator.

In some cases, no (proper) transition point could be determined. In such cases, no clear peak was visible in the derivative of the measured signal. In most cases, the experiment ended (because

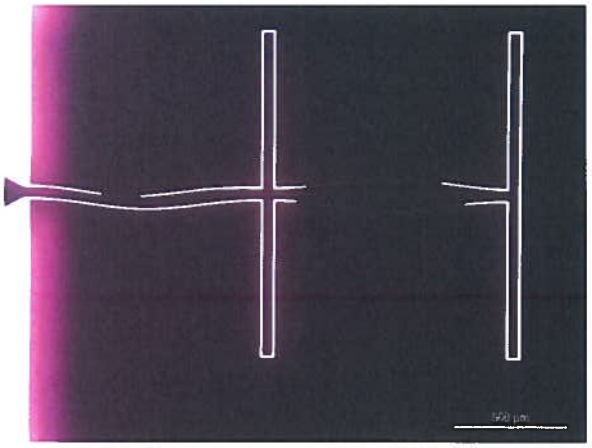

Figure 5.1: Part of chip showing fabrication errors. The lines of the sensor are not straight and the trench between sensor and actuator is not fully edged.

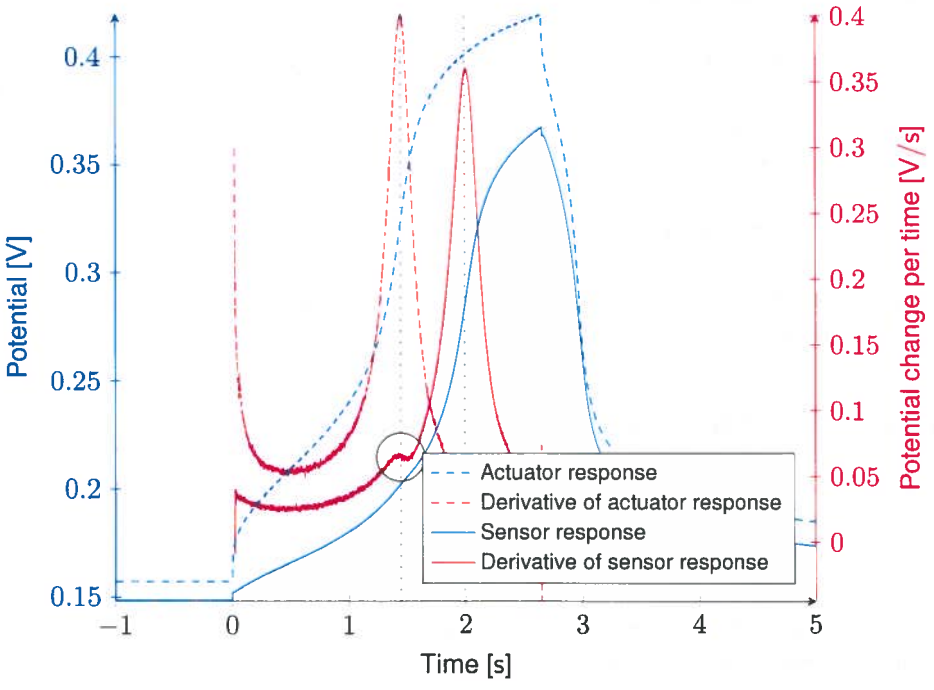

Figure 5.2: Example of an obtained chronopotentiogram from both sensor (solid blue line) and actuator (dashed blue line), with distance d of 5 µm and sensor line width w of 5 µm, after a current density of 10 A/m² is applied at time $t > 0$. The solution contained 3 mM KCl and 0.5 M KNO_3. Derivatives of the (filtered) responses are shown for reference in red. The detected transition times are indicated by the black dotted lines. The circle indicates a small peak in the derivative, likely the result of a resistive connection through the solution between the two electrodes.

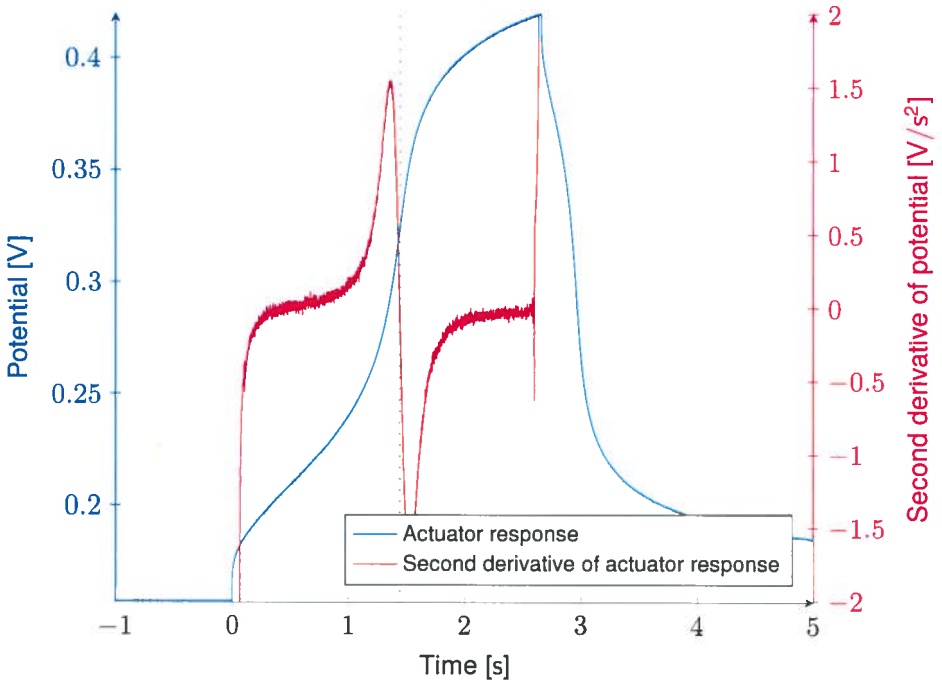

Figure 5.3: Example of an obtained chronopotentiogram from the actuator (solid blue line), equal to the one in Figure 5.2 after a current density of $10\,A/m^2$ is applied at time $t > 0$. The solution contained 3 mM KCl and 0.5 M KNO_3. The (filtered) second derivative of the actuator signal is shown in red. The detected transition time is indicated by the black dotted lines.

of the potential limit set on the actuator signal to prevent oxidation of the actuator) before a transition occurred at the sensor. Data points which are not based on a clear inflection point (peak in the derivative of the signal) as a result of a false detection by the MATLAB script in Listing E.5 of Appendix E, are omitted in the data plots in this chapter. False detections occur because the script looks at the maximum value of the derivative to find the peak and there will always be a highest value. False detection are clearly visible as the resulting transition time is either equal to the length of the current pulse or much lower than the transition time as observed at the actuator.

In Subsection 2.1.2, it was shown that a root at $t = \tau/4$ should be visible in the second derivative of the measured potential. Figure 5.3 shows the actuator response of Figure 5.2 with its (filtered) second derivative. As can be seen in this figure, the derivation is even after filtering (running average) quite noisy. As the graph is rather flat around $t = \tau/4 \approx 0.35$ s, the root cannot be clearly determined. Although theoretically the detection of this root would mean faster detection and no oxide formation on the actuator, it does not seem feasible with the current setup and is therefor not further analyzed in the remaining sections.

5.3 Calibration curve

The sensor-actuator system is first characterized by measuring the response for different Cl^- concentration levels. For reliable measurement results, for each Cl^- concentration level, the chronopotentiometric measurement was performed twice, after the solution was stirred in between to assure a constant Cl^- concentration throughout the solution. After the series of 1 mM to 6 mM KCl in a solution also containing 0.5 M KNO_3 was performed, the procedure was repeated using the same chip. The resulting calibration curves are visible Figure 5.4.

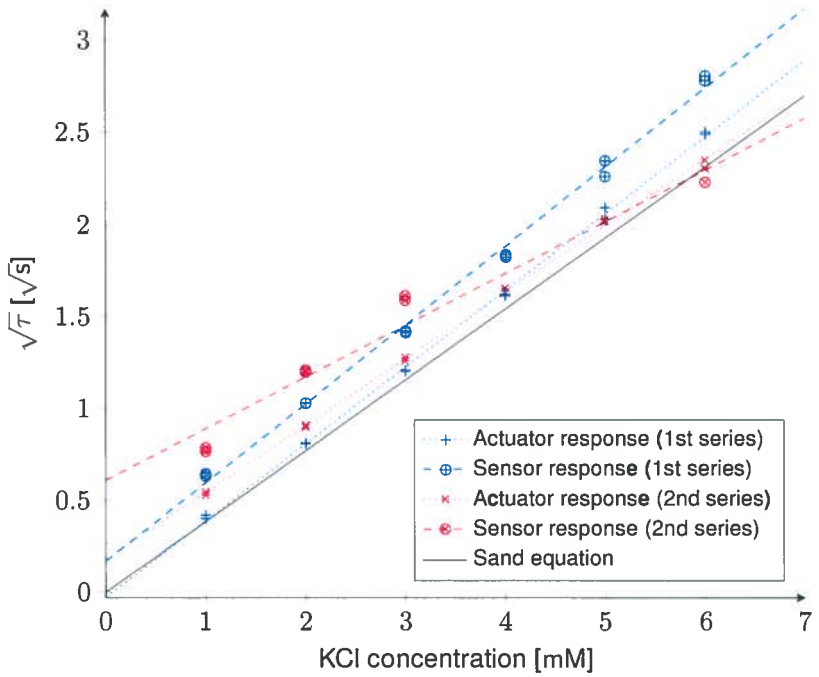

Figure 5.4: Calibration curves of a sensor-actuator system. Two measurements were conducted for each KCl concentration in the range 1 mM to 6 mM with a background electrolyte of 0.5 M KNO_3. The measurement series was then repeated for KCl concentrations in the same range. The used sensor-actuator system has $d = 5\,\mu m$ and $w = 5\,\mu m$ and a current density of 10 A/m^2 was used.

As visible in the figure, the second measurement series shows big derivations compared to the first measurement series, especially for later measurements (as the series were performed by increasing the KCl concentration levels, results for higher concentration were obtained later in time). In the second measurement series, no valid inflection points were found in the sensor response for Cl^- concentration levels of 4 mM and 5 mM. Also the transition time value of the sensor for 6 mM in this series has a problem, as it was detected earlier than the transition time at the actuator. Since the actuator should be causing the concentration change at the sensor (and thus the inflection point in the observed potential of the sensor electrode), this must be a false detection. While observing the original chronopotentiogram and its derivative, it was noted that the derivative only showed a very small peak, similar to the first peak in the derivative of the sensor response in Figure 5.2 and not a large peak as is common for a proper detection.

Since the results later in time are not always detected, some doubts arise on the stability of the system, which is further investigated in Section 5.8. The results of the measurements with different values for d and w in the following sections are compared with the calibration curve based on the first measurement series as these results are less questionable.

The actuator response is very close to the theoretical curve. Based on the linear fit of the data of the actuator in the first measurement series, a diffusion coefficient of 2.38 m/s^2 is observed, if all other values, such as the area, are supposed to be as designed. This value is slightly above the reported value of 2.03 m/s^2 found in literature [13]. However, the area of the electrode is not very well defined, as surface roughness might increase the effective area, which would lower the used current density (as a constant current is applied by the potentiostat) and as a result from the Sand equation (Equation 2.17) change the slope.

The one-dimensional model of Section 2.2 is clearly insufficient to describe the sensor response.

Although the separated sensor-actuator approach indeed results in a concentration dependent measurement signal, there is an offset between the transition times observed at the actuating and sensing electrodes, which was not predicted by the model. This time offset is increasing for higher concentration (note that Figure 5.4 shows the square root of the transition time instead of the transition time itself), and is therefore at least partially dependent on the Cl^- ion concentration.

To explain the difference between the model and the measured results, the structure of the sensor-actuator system has to be closely observed. In the model, the inflection point is the result of a change in the slope of the concentration gradient as a result of the change from a constant current carried by the Cl^- ions to a decreasing current, when a second redox couple also delivers part of the electron flow (refer to Subsection 2.2.1). In this case, it was assumed that the diffusion profile extends perpendicular to the (infinite) planar actuator surface and the sensor is positioned in the face of this surface. However, in the fabricated chip design, the sensor is positioned at the edges of the planar electrode and the diffusion profile will be more circular.

Another assumption made in the model is that only the initial redox couple (in this c se the reaction $Cl^- + Ag \rightarrow AgCl + e^-$) is influencing the potential of the sensor. However, Figure 5.2 shows a signal shape very similar to the signal of the actuator, which is influenced not only by the initial redox couple, but also by a second one, which causes the leveling of the signal. The likelihood of a resistive path between sensor and actuator (refer to Section 5.2) makes it more difficult to determine exactly what the transition at the sensor is caused by.

The exact mechanism responsible for the sensor signal is therefore unclear. Probably a mixture of the exact shape of the diffusion profile and a mixed potential at the electrode due to multiple redox couples being present causes the shift of the inflection point.

5.4 Influence of sensor size

One of the design variables is the line width w of the sensor as presented in Section 3.1. Three chip designs were fabricated in which the line width was varied. Unfortunately, no chips with the largest line width (Design 3, $w = 50\,\mu m$), could be used due to fabrication errors such as sensor deformations, other damages such as scratches and non evenly deposited AgCl.

The same measurement series as was done for the calibration curves of Section 5.3 was repeated using a chip with $w = 20\,\mu m$ (Design 2). For reliable measurement results, for each Cl^- concentration level, the chronopotentiometric measurement was performed twice, after the solution was stirred in between to assure a constant Cl^- concentration throughout the solution. The resulting curve is plotted together with the response of the chip with smaller line width ($w = 5\,\mu m$) in Figure 5.5.

A number of features stand out in the figure. First of all, the transition times for the actuator with $w = 20\,\mu m$ are later than expected. Since the current densities are equal, the response should be closer to the curve for the Sand equation (Equation 2.17). Why this shift occurs is unclear. Based on the figure, one would expect that the concentration of KCl in the used solution was off, however the same stock solution was used for both chips with $w = 5\,\mu m$ and $w = 20\,\mu m$.

Another observation is the increase in the difference between the transition time of the sensor and the transition time for the actuator for larger sensors (higher w). This behavior might be caused by the time it takes for the lowered Cl^- concentration (as a result of the current running through the actuator) to diffuse over the sensor. Since the sensor surface is larger, it takes more time before the concentration at the sensors surface reaches a lower value, i.e. the concentration nearer to the actuator (at the edges of the sensor) will be lower than the concentration at the center of the sensor.

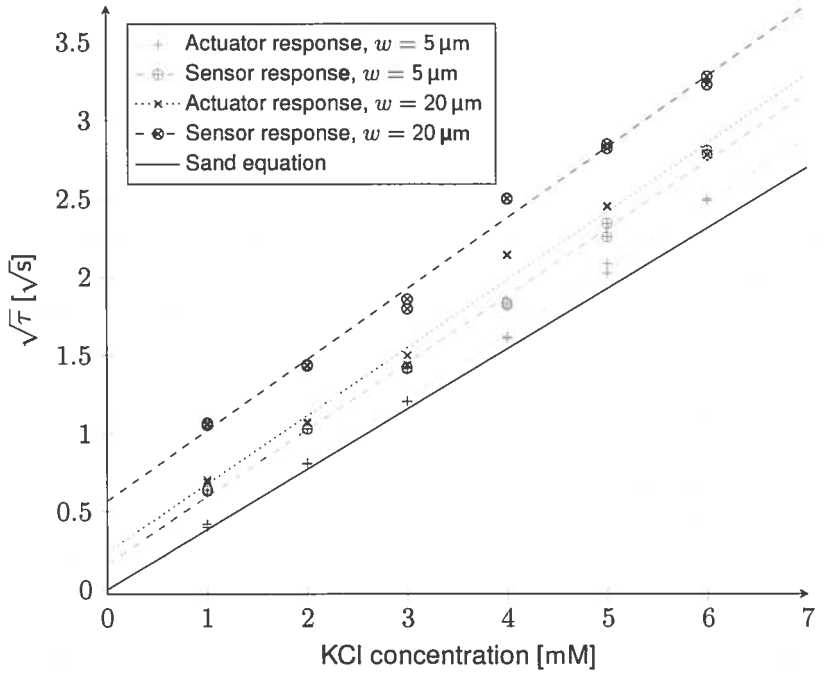

Figure 5.5: Influence of sensor size on the transition time measurements of a sensor-actuator system. Two measurements were conducted for each KCl concentration in the range 1 mM to 6 mM with a background electrolyte of 0.5 M KNO_3. The sensor-actuator system had $d = 5\,\mu m$ and $w = 20\,\mu m$ and a current density of $10\,A/m^2$ was used. For comparison, the results of a sensor-actuator system with $d = 5\,\mu m$ and $w = 5\,\mu m$ are included in the graph.

The observed sensor potential is the result of a mixed potential across the sensor surface and takes longer to reach the inflection point typical for the transition time.

5.5 Influence of distance between sensor and actuator

Besides line width w, also the distance d between the sensor and actuator can be varied in size. For this purpose, a chip with $d = 15\,\mu m$ (Design 4) was fabricated to compare it with the chip used in Section 5.3, which had $d = 5\,\mu m$.

The calibration procedure was repeated with this chip, i.e. a series of two measurements of a solution with KCl in the range of 1 mM to 6 mM in 1 mM steps and a background electrolyte of 0.5 M KNO_3. A current density of $10\,A/m^2$ was used. Figure 5.6 shows the resulting calibration curve combined with the calibration curve of Section 5.3 for comparison.

Just as was the case in the previous section, the transition times observed at the actuator are higher than expected. Also in this case it is unclear where this shift originates. The same stock solutions were used as in the previously presented measurement results, so the KCl concentration should be the same. In Section 5.8, the transition times at the actuator are further investigated.

The observed sensor signals did not result in a transition time detection for every measurement. In these cases, no inflection point was reached before the current pulse was ended to prevent further oxidation of the actuator. The larger distance between sensor and actuator gives more chance for unwanted effects, such as convection, to occur.

In the cases where a successful detection was possible, an increase in the time between the transition at the actuator and sensor as compared to the chip with smaller d is observed. Because

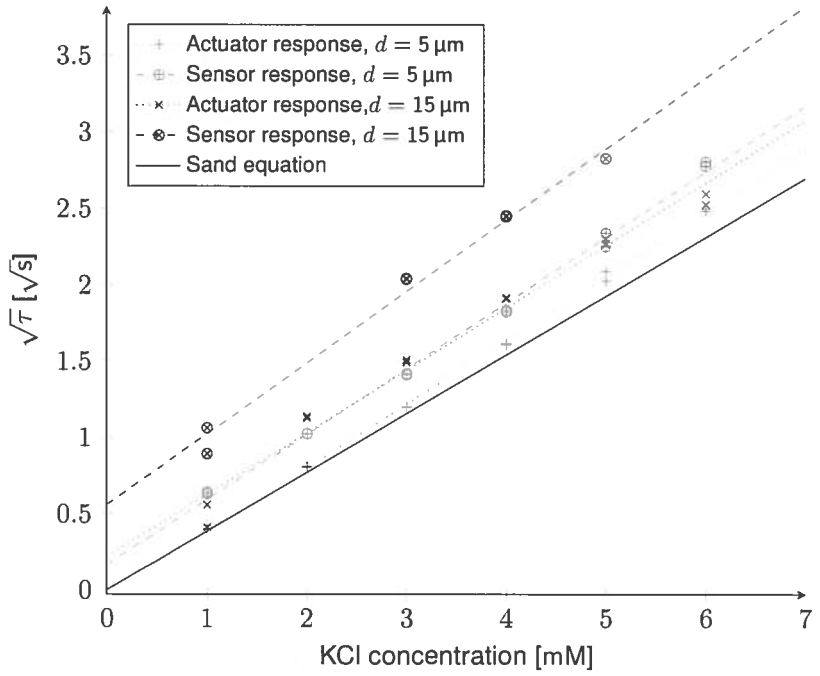

Figure 5.6: Influence of distance d between sensor and actuator. Two measurements were conducted for each KCl concentration in the range 1 mM to 6 mM with a background electrolyte of 0.5 M KNO_3. The sensor-actuator system had $d = 15\,\mu m$ and $w = 20\,\mu m$ and a current density of 10 A/m^2 was used. For comparison, the results of a sensor-actuator system with $d = 5\,\mu m$ and $w = 5\,\mu m$ are included in the graph.

of this increase in time, it is likely that the delay between sensing a transition at the actuator and sensing it at the sensor is diffusion controlled; i.e. it takes time for the concentration change to reach the sensor as the distance d between the two has to be covered first.

5.6 Influence of current density level

According to the Sand equation (Equation 2.17), the transition time is dependent on the current density. To verify the behavior of the sensor-actuator system for different current densities, measurements are performed with a chip with $w = 5\,\mu m$ and $d = 5\,\mu m$ in a solution containing 3 mM KCl and 0.5 M KNO_3, while varying the current density from 3 A/m^2 to 10 A/m^2 in 1 A/m^2 steps. For each current density, the measurement was repeated after stirring the solution.

By rearranging the Sand equation (Equation 2.17), a linear relation between the square root of τ and one over the current density ($1/J = A/I$) can be obtained:

$$\sqrt{\tau} = \frac{nFAC^*_{red}}{I}\sqrt{\frac{D_{red}\pi}{4}} = \frac{1}{J}nFC^*_{red}\sqrt{\frac{D_{red}\pi}{4}} \tag{5.1}$$

Figure 5.7 shows the obtained transition times for the different current densities. Figure 5.8 shows the curve resulting from the current density variation, plotted in such a way that a linear relation should be visible (Equation 5.1).

As was also noted in previous sections, in this measurement series the transition time observed at the actuator is higher than would be expected by the Sand equation, which is most visible in Figure 5.7. Figure 5.8 shows that the actuator response follows the expected dependence on current density. By changing the current density, the sensitivity of the system can be changed, since the

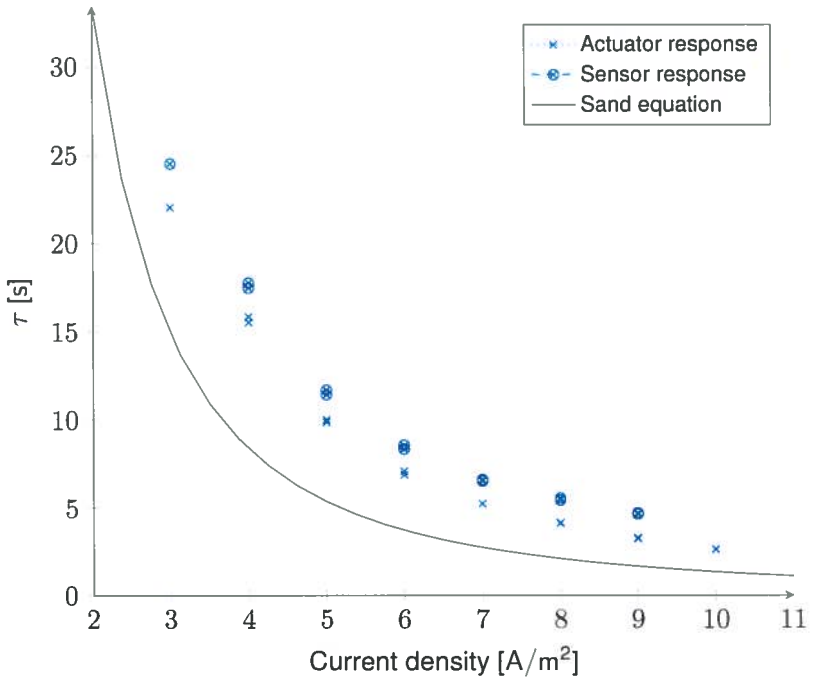

Figure 5.7: Influence of current density on measured transition times. Two measurements were conducted for each current density in the range of 3 A/m² to 10 A/m² in a solution containing 3 mM KCl and 0.5 M KNO_3. The used sensor-actuator chip had $d = 5$ µm and $w = 5$ µm.

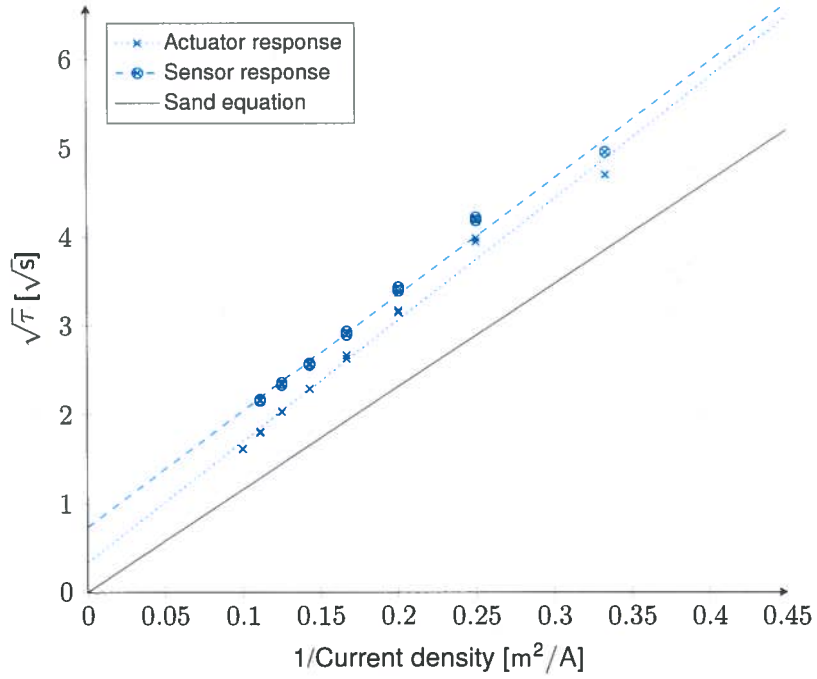

Figure 5.8: Influence of current density on measured transition times. The same measurements as in Figure 5.7, but now plotted as the square root of transition time versus the reciprocal of the current density. Two measurements were conducted for each current density in the range of 3 A/m² to 10 A/m² in a solution containing 3 mM KCl and 0.5 M KNO_3. The used sensor-actuator chip had $d = 5$ µm and $w = 5$ µm.

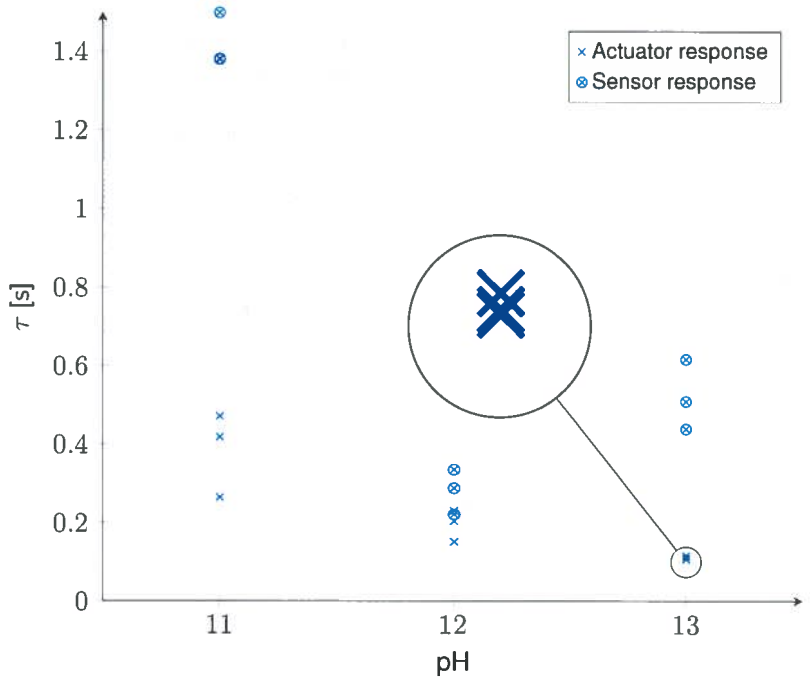

Figure 5.9: Influence of pH-level on the transition time measurements. Three measurements were conducted for each pH-level in the reage from 11 to 13 in steps of 1. A chip with $w = 5\,\mu m$ and $d = 15\,\mu m$ was used in a solution which contained, besides KOH 1 mM KCl and 1 M KNO_3. A current density of $10\,A/m^2$ was applied to the actuator electrode.

transition time can be shifted by applying a different current density, i.e. making sure that the transition time occurs within a certain time frame. However, there is a deviation from the Sand equation, which was also observed in the previous sections.

5.7 Influence of pH-level

The Ag/AgCl electrode is known to be sensitive to OH^- ions, although with a much lower sensitivity coefficient (refer to Subsection 2.1.3). To see the influence of the hydroxide ion, measurements are performed in a solution consisting of 1 mM KCl, 1 M KNO_3 and a KOH concentration corresponding to pH-levels of 11, 12 and 13. The used chip had $w = 5\,\mu m$ and $d = 15\,\mu m$. Refer to Table 5.1 for the OH^- concentration corresponding to these pH-levels and the equivalent concentration, defined as the OH^- concentration multiplied by the sensitivity coefficient. If the equivalent concentration gets near the Cl^- concentration, influencing of the measurements is expected.

Table 5.1: Concentration of OH^- ions for the pH-levels used in Figure 5.9. The equivalent concentration is defined as the OH^- concentration multiplied by the sensitivity coefficient.

pH	OH^- concentration [mM]	Equivalent concentration [mM]
11	1	0.024
12	10	0.24
13	100	2.4

Figure 5.9 shows the detected transition times resulting from the pH variation. The values found for pH=11 are very similar to the values seen in Figure 5.6 for the same chip design (although another

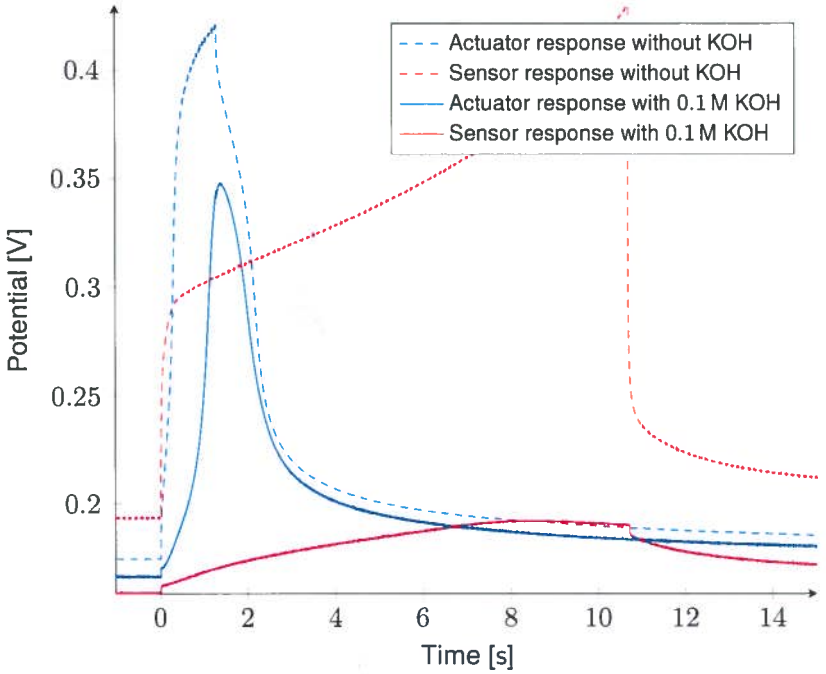

Figure 5.10: Influence of pH-level on the transition time measurements. Three measurements were conducted for each pH-level in the range of 11 to 13 in steps of 1. A chip with $w = 5\,\mu m$ and $d = 15\,\mu m$ was used in a solution which contained, besides KOH 1 mM KCl and 1 M KNO_3. A current density of 10 A/m^2 was applied to the actuator electrode.

physical chip was used) with $w = 5\,\mu m$ and $d = 15\,\mu m$. However, for higher pH, the transition time measurement is heavily affected, just as was predicted by the theory since the equivalent concentration is getting near the Cl^- ion concentration. The results of Figure 5.9 confirm that the selectivity coefficient k_{Cl^-,OH^-} should be in the order of 1×10^{-2}, as was the reported value of Umezawa [12].

The determined transition times for higher concentrations are no longer corresponding to the Cl^- ion concentration. As can be seen in Figure 5.10, the shape of the observed potential (due to the applied current pulse) has changed considerably. The potential at the actuator quickly goes up to a first plateau and then slowly increases further, until the experiment is ended to prevent oxidation of the actuator surface. The detected transition times for the higher pH-levels are consequently low, as there is a transition just after the start of the experiment. The sensor response does not show a clear inflection point, which results in less reliable detections, visible by a large spread of the transition time for the sensor at pH=13 in Figure 5.9.

5.8 Stability

Since the repeatability of the first experiment seemed lacking, more research was done on the stability of the used sensor-actuator system. After the experiments of Section 5.3, the used chip was inspected under a microscope. As can be seen in Figure 5.11, the edges of the actuator are colored lighter, which is likely due to more redox conversion at these areas of the actuator. Although it was assumed that the diffusion profile extends into the solution perpendicularly with respect to the electrode, at the edges it is clearly visible that this is not the case.

Assuming that the potential of the electrode is equal across the electrode surface, the edges

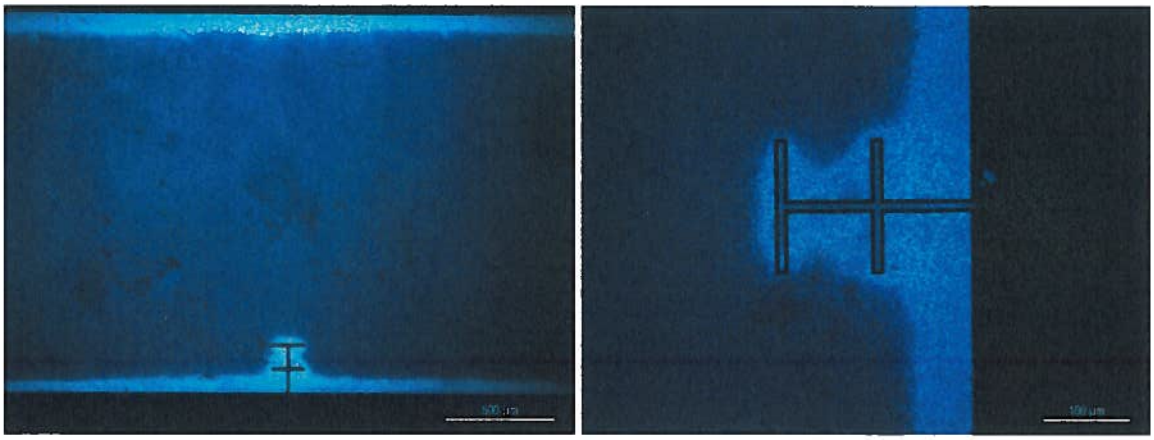

(a) (b)

Figure 5.11: Photograph of the chip used for the measurements of Figure 5.4. The edges of the actuating electrode show discoloration. (a) Large portion of the actuator (left and right edges not visible). (b) Close-up of sensing electrode.

attract Cl^- ions more easily than electrode surface areas further away from the edges. This could result in locally higher current densities and thus more conversion from Cl^- to AgCl. As in this case the AgCl thickness increases near the edges, at the diffusion of Ag towards the electrode surface will take more time, and the area will consume Cl^- at a lower rate. At this point, the edge is effectively moved more inward. As the sensing electrode is located at the edge of the actuator, this means that d is effectively increased, and thus the local ion concentration at the sensor is less influenced by the actuator.

To further investigate the stability of the fabricated sensor-actuator system, a series of measurements were done in the course of one day, while keeping the chip ($w = 5\,\mu m$ and $d = 5\,\mu m$) immersed in a solution containing 3 mM KCl and 0.5 M KNO_3. Figure 5.12 shows a plot of the resulting observed transition times at both the sensing and actuating electrode accompanied by a table showing the start times of the measurements relative to the first measurement.

A surprising observation of Figure 5.12 is that the transition time increases over time. This could be explained by the evaporation of water in the solution, leaving a solution with a higher Cl^- ion concentration. The open circuit voltage, measured just before the current pulse is applied, confirms this hypothesis as the difference between the first and last measurement indicates almost a doubling in concentration. A similar experiment within the BIOS group with a normal chronopotentiometric setup (sensor and actuator combined in one electrode) did not show this behavior, but in this case every day a few measurements were taken, each time using a fresh solution.

An observation made in the previous sections is the offset of the actuator response from the Sand equation (Equation 2.17) and different slopes in the $\sqrt{\tau}$ versus concentration plots. To investigate this offset some more, the actuator responses of the three chips used in the calibration curve (Section 5.3), the larger sensor size (Section 5.4) and the larger distance between sensor and actuator (Section 5.5) are grouped into Figure 5.13.

As can be seen in the figure, there is a variation in slopes. However, due to the low amount of measurements and the small range, it is unclear if these are (random) measurement errors or systematical errors. The used detection script, visible in Appendix E, also introduces some shifts in τ due to filtering of the derivative. Thirdly some errors could have occurred due to small concentration deviations between the calculated and actual concentration levels. Besides that, the temperature

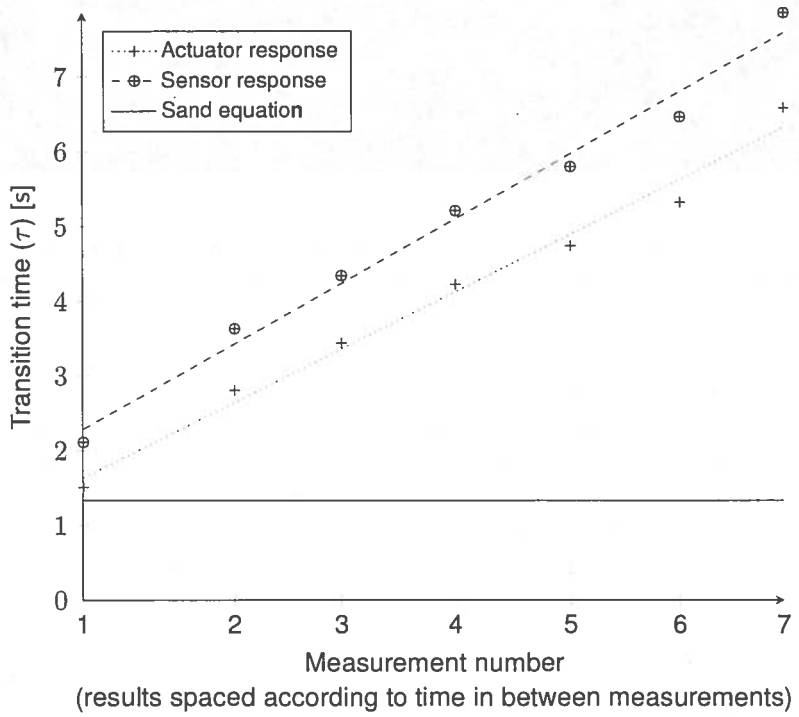

Measurement number	Start time of measurement [hh:mm:ss]	Open circuit voltage [V]
1	00:00:00	0.153
2	01:22:09	0.144
3	02:20:28	0.143
4	03:22:43	0.141
5	04:25:25	0.139
6	05:25:15	0.138
7	06:21:47	0.136

Figure 5.12: Measurement of drift over time. Seven measurements were conducted with a sensor-actuator system with $d = 5\,\mu m$ and $w = 5\,\mu m$ in a solution containing 3 mM KCl and 0.5 M KNO_3 using a current density of $10\,A/m^2$. The table shows the starting time of each measurement relative to the first one and the open circuit voltage measured by the actuator, just before the experiment.

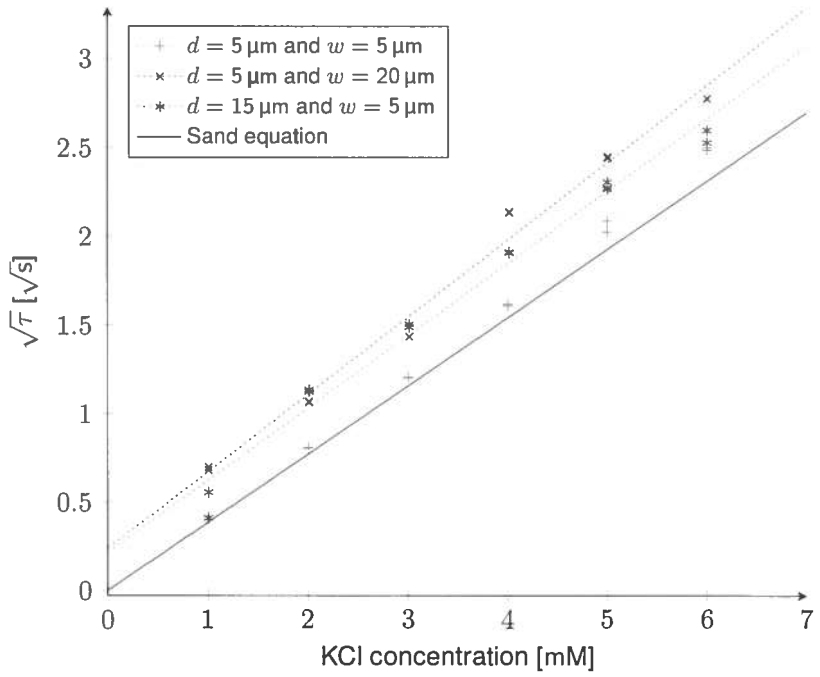

Figure 5.13: Comparison of actuator response for different chips. The actuator responses of the chips used in Sections 5.3, 5.4 and 5.5 are plotted in one figure. In all three experiments, a background electrolyte containing 0.5 M KNO_3 and a current density of 10 A/m^2 was used while the KCl concentration varied from 1 mM to 6 mM.

within the lab is not well controlled and evaporation during the course of a measurement series (upto an hour) could also affect the measurements.

5.9 Summary

The fabrication process resulted in a number of working chips, although some showed defects. The experiments showed a resistive path between the sensor and actuator signal. During the measurements, the transition times were determined using a MATLAB script. In some cases this resulted in wrong results.

In this chapter, calibration curves for different separated sensor-actuator systems were compared. In these experiments, the size of the sensor (through line width w) and the distance (d) between sensor and actuator were varied. Both a larger sensor and a larger distance resulted in a larger time delay between the transition time at the actuator and the transition time at the sensor. Also the current density applied to the actuator was varied. The transition time varied as expected with this current density. By adding KOH, the pH was varied. For pH>11, proper transition time measurements were no longer possible as an additional transition point is introduced.

Comparing the obtained calibration curves of the actuators on the different chips showed a spread in measurement results. It is not clear where these shifts originate, but possible causes are the used detection script, random errors not counteracted by statistical data (because of the low amount of measurements) and a shifted concentration level in the used solutions.

6 Conclusion & recommendations

6.1 Conclusion

The aim of this project was to give a proof of concept for a chronopotentiometric system with separated sensing and actuating electrodes. The performed experiments show that the sensor indeed senses the local concentration changes resulting from the current applied to the actuator. A linear relation between concentration and the square root of the transition time was observed at the actuator, just as predicted by the Sand equation (Equation 2.17). The sensor showed the same linear relation, but an addition delay was observed between the sensor and actuator signal.

The variation of design parameters resulted in a few observations. First of all, the distance (d) between the two electrodes should be small. A larger distance resulted in less proper detections of the transition time and an increase in the delay between the transition time at the sensor and actuator. Secondly, a larger sensor area (by increasing line width w) resulted in an increase of the transition time as observed at the sensor.

Variation of the applied current density resulted in a change of the transition time. This follows the Sand equation (Equation 2.17) and and could be used to tune the sensitivity of the sensor-actuator system by changing the current density in such a way that the transition time always falls within a certain time frame as increasing the current density results in a decrease of the transition time and vice versa.

Using the sensor-actuator system in a solution with high pH-level (above pH=11) prevented the system from functioning properly as the OH^- ions interfere with the Cl^- ion sensing at the Ag/AgCl electrodes. Theory predicted this behavior and it was confirmed that the selectivity coefficient for OH^- ions as the interferent for Cl^- ions should be in the order of 1×10^{-2}.

After a number of experiments, the actuating electrode showed discoloration at the edges. This is the result of more ion conversions taking place at these edges, as it is easier to attract Cl^- ions in these regions. Due to this effect, the edges become passivated after a while, effectively moving the edge more inward and increasing the distance d between sensor and actuator.

A one dimensional model was presented to describe the diffusion profile perpendicularly extending into the solution from the surface of the actuating electrode. However, the model could not be verified as the sensor was positioned adjacent to the actuator.

6.2 Outlook

For further research, a few areas of interest can be formulated. The current work could benefit from more data to perform the analysis on data that is more statistically sound. A larger concentration range for the calibration curves could give more insight into the correspondence with the Sand equation, however, too high concentrations lead to either a high transition time, making it difficult to prevent convection from interfering, or high current densities, quickly damaging the actuating electrode.

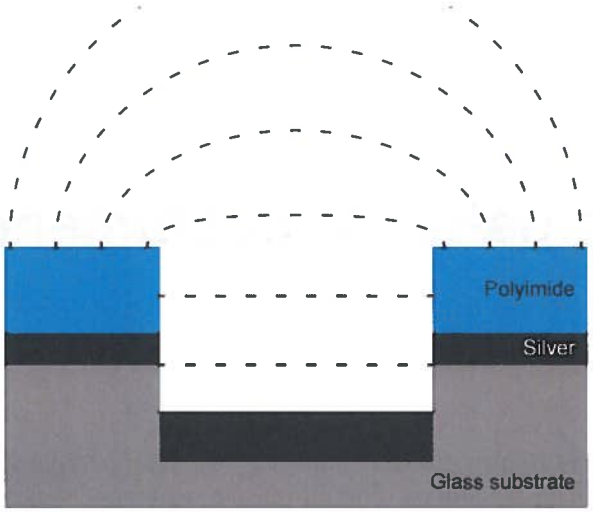

Figure 6.1: Simplified cross-section of a possible design for a sensor-actuator system which ensures a uniform diffusion profile over the actuator. The (black) electrode at the bottom of a recess in the substrate acts as the actuator. Because of the recess, the diffusion profile (indicated by the dashed lines) extends linearly into the solution to the top of the recess, before a more circular profile will form. The sensor is placed around the trench to sense the concentration changes resulting from the actuation.

Experiments should be focused on using chips with a small distance between sensor and actuator, as a larger distance yielded less proper detections of the transition time. It would also be interesting to see whether chips with larger sensor area behave similarly as was observed in the experiments in this work. This work presented a chip design for this (Design 3), however no chips of this type were successfully fabricated during this project. After new wafers will be produced, additional experiments with these chips should be possible.

The deposition of AgCl is not extensively studied during this project, but could be an interesting production parameter for further improvements. The thickness of the AgCl layer might be a factor in the number of experiments that can be performed before the edge effect at the actuator becomes too pronounced and starts influencing the sensor signal. Also, the number of measurements that a chip can withstand could possibly be increased by reversing the redox reaction, converting AgCl into Cl^- and Ag, effectively cleaning the actuator.

6.3 Recommendations

The largest benefit of the separated sensor-actuator approach, no electrochemical fouling of the sensor, is partly voided by the fact that fouling of the actuator still influences the sensor signal in the current design. The actuator signal itself did show the expected dependence on concentration level and the ohmic drop resulting from the current flow trough the electrode did not prevent the detection of the transition time. Therefor, in future studies on the detection of chloride with a focus on long term measurements, the conventional chronopotentiometric approach might be very suitable.

In case the separated approach is more suitable for a specific application, the chip should be redesigned in such a way that the diffusion profile is uniform over the full actuator, to prevent localized surface alterations. An example of such a design is given in Figure 6.1. In this design, the actuator is put at the bottom a recess in the substrate to ensure a linear diffusion profile extending perpendicularly from the actuator into the solution. The sensor is put at the wall of this recess to observe the concentration changes resulting from the actuation. The resulting observations should be more in line with the model presented in this work.

References

[1] G. Loreto, M. Di Benedetti, R. Iovino, A. Nanni, and M. A. Gonzalez-Nunez, "Evaluation of corrosion effect in reinforced concrete by chloride exposure," in *SPIE 7983, Nondestructive Characterization for Composite Materials, Aerospace Engineering, Civil Infrastructure, and Homeland Security 2011*, H. F. Wu, Ed., vol. 7983, Mar. 2011, pp. 79 830A–79 830A–10. doi:10.1117/12.880156

[2] M. Montemor, A. Simões, and M. Ferreira, "Chloride-induced corrosion on reinforcing steel: from the fundamentals to the monitoring techniques," *Cement and Concrete Composites*, vol. 25, no. 4-5, pp. 491–502, May 2003. doi:10.1016/S0958-9465(02)00089-6

[3] Y. Abbas, W. Olthuis, and A. van den Berg, "A chronopotentiometric approach for measuring chloride ion concentration," *Sensors and Actuators B: Chemical*, Jul. 2013. doi:10.1016/j.snb.2013.07.046

[4] A. J. Bard and L. R. Faulkner, *Electrochemical Methods: Fundamentals and Applications*, 2nd ed. Wiley, 2001.

[5] W. Olthuis, "Syllabus Biomedical Signal Acquisition (191210720)," 2012.

[6] W. Olthuis, *Measurement of Chemical Quantities*, P. P. L. Regtien, F. van der Heijden, and M. J. Korsten, Eds. Kogan Page Science, 2004. doi:10.1016/B978-190399658-4/50010-1

[7] E. Bakker, V. Bhakthavatsalam, and K. L. Gemene, "Beyond potentiometry: robust electrochemical ion sensor concepts in view of remote chemical sensing." *Talanta*, vol. 75, no. 3, pp. 629–35, May 2008. doi:10.1016/j.talanta.2007.10.021

[8] P. Bergveld, J. Eijkel, and W. Olthuis, "Detection of protein concentrations with chronopotentiometry," *Biosensors and Bioelectronics*, vol. 12, no. 9-10, pp. 905–916, Nov. 1997. doi:10.1016/S0956-5663(97)00023-7

[9] G. J. Janz and D. J. G. Ives, "Silver, silver chloride electrodes," *Annals of the New York Academy of Sciences*, vol. 148, no. 1 Bioelectrodes, pp. 210–221, Feb. 1968. doi:10.1111/j.1749-6632.1968.tb20350.x

[10] F. L. Almeida, M. Bariatto Andrades Fontes, C. Jimenez, and I. Burdallo, "Secondary Ag/AgCl Pseudo-Reference Electrode on Silicon Substrate," in *ECS Transactions*, vol. 14, no. 1. ECS, 2008, pp. 73–82. doi:10.1149/1.2956019

[11] U. Angst, B. Elsener, C. K. Larsen, and Ø. Vennesland, "Potentiometric determination of the chloride ion activity in cement based materials," *Journal of Applied Electrochemistry*, vol. 40, no. 3, pp. 561–573, Oct. 2009. doi:10.1007/s10800-009-0029-6

[12] Y. Umezawa, *CRC handbook of ion-selective electrodes: selectivity coefficients*. Boca Raton, FL: CRC Press, 1990.

[13] E. L. Cussler, *Diffusion: Mass Transfer in Fluid Systems*, 2nd ed. Cambridge Cambridge University Press, 1997.

[14] B. van der Schoot and P. Bergveld, "An ISFET-based microlitre titrator: integration of a chemical sensor-actuator system," *Sensors and Actuators*, vol. 8, no. 1, pp. 11–22, Sep. 1985. doi:10.1016/0250-6874(85)80020-2

[15] W. Olthuis and P. Bergveld, "Integrated coulometric sensor-actuator devices," *Mikrochimica Acta*, vol. 121, no. 1-4, pp. 191–223, 1995. doi:10.1007/BF01248251

A Derivation of Equation 2.14

This appendix shows all the steps needed to do the derivation of Equation 2.14 in Section 2.1.2. All the boundary conditions of Section 2.1.2 are repeated here:

$$\frac{\delta C_{red}(x,t)}{\delta t} = D_{red}\left[\frac{\delta^2 C_{red}(x,t)}{\delta x^2}\right] \tag{A.1}$$

$$C_{red}(x,0) = C^*_{red} \tag{A.2}$$

$$\lim_{x\to\infty} C_{red}(x,t) = C^*_{red} \tag{A.3}$$

$$D_{red}\left[\frac{\delta C_{red}(x,t)}{\delta x}\right]_{x=0} = \frac{i(t)}{nFA} \tag{A.4}$$

This appendix uses the following notation to indicate a Laplace transformed function:

$$\bar{f}(s) = \mathcal{L}\{f(t)\}$$

For clarity, the symbol u is introduced below as argument of the Laplace transformation with respect to x, to discriminate between the argument s from the Laplace transformation with respect to t used before. Thus, the Laplace transform of a function f in x is given by:

$$\bar{f}(u) = \mathcal{L}\{f(x)\}$$

First, Equation A.2 is Laplace transformed with respect to time and rearranged:

$$s\bar{C}_{red}(x,s) - C_{red}(x,0) = D_{red}\left[\frac{\delta^2 \bar{C}_{red}(x,s)}{\delta x^2}\right] \tag{A.5}$$

$$\frac{\delta^2 \bar{C}_{red}(x,s)}{\delta x^2} - \frac{s}{D_{red}}\bar{C}_{red}(x,s) = -\frac{C^*_{red}}{D_{red}} \tag{A.6}$$

To make notation easier, Equation A.6 is written as:

$$\frac{\delta^2 f(x)}{\delta x^2} - \alpha^2 f(x) = -\beta \tag{A.7}$$

with:

$$f(x) = \bar{C}_{red}(x,s) \tag{A.8}$$

$$\alpha^2 = \frac{s}{D_{red}} \tag{A.9}$$

$$\beta = \frac{C^*_{red}}{D_{red}} \tag{A.10}$$

Equation A.7 is of a standard form and can be easily transformed [4, p. 773]:

$$u^2\bar{f}(u) - uf(0) - \left[\frac{df(x)}{dx}\right]_{x=0} - \alpha^2\bar{f}(u) = -\frac{\beta}{u} \tag{A.11}$$

Rearranging Equation A.11 results in:

$$\bar{f}(u)\left(u^2-\alpha^2\right) = -\frac{\beta}{u} + uf(0) + \left[\frac{df(x)}{dx}\right]_{x=0} \tag{A.12}$$

$$\bar{f}(u) = \frac{-\frac{\beta}{u} + uf(0) + \left[\frac{df(x)}{dx}\right]_{x=0}}{u^2-\alpha^2} \tag{A.13}$$

$$= \frac{-\beta + u^2f(0) + u\left[\frac{df(x)}{dx}\right]_{x=0}}{\left(u^2-\alpha^2\right)u} \tag{A.14}$$

$$= \frac{-\beta + u^2f(0) + u\left[\frac{df(x)}{dx}\right]_{x=0}}{(u+\alpha)(u-\alpha)u} \tag{A.15}$$

$$= \frac{A(s)}{u+\alpha} + \frac{B(s)}{u-\alpha} + \frac{\Gamma(s)}{u} \tag{A.16}$$

Since A, B and C_{red} might contain α, they can be functions of s.

To yield $\Gamma(s)$, all terms in Equations A.15 and A.16 are multiplied by u:

$$\frac{-\beta + u^2f(0) + u\left[\frac{df(x)}{dx}\right]_{x=0}}{(u+\alpha)(u-\alpha)} = \frac{uA(s)}{u+\alpha} + \frac{uB(s)}{u-\alpha} + \Gamma(s) \tag{A.17}$$

Afterwards, u is set to 0, resulting in:

$$\Gamma(s) = \frac{\beta}{\alpha^2} \tag{A.18}$$

Inserting Equation A.18 into Equation A.16 and using the inverse Laplace transform yields:

$$f(x) = \frac{\beta}{\alpha^2} + A(s)e^{-\alpha x} + B(s)e^{\alpha x} \tag{A.19}$$

Putting Equation A.8 in Equation A.19 forms:

$$\bar{C}_{red}(x,s) = \frac{\beta}{\alpha^2} + A(s)e^{-\alpha x} + B(s)e^{\alpha x} \tag{A.20}$$

Equation A.3 can be transformed to:

$$\lim_{x\to\infty} \bar{C}_{red}(x,s) = \frac{C^*_{red}}{s} \tag{A.21}$$

To comply to the boundary condition of Equation A.21, $B(s)$ in Equation A.20 must be zero since the limit of $e^{\alpha x}$ for $x \to \infty$ goes to infinity (assuming $\alpha > 0$).

Solving for $A(s)$ is done by multiplying all terms in Equations A.15 and A.16 by $(u+\alpha)$:

$$A(s) + \frac{B(s)(u+\alpha)}{u-\alpha} + \frac{\Gamma(s)(u+\alpha)}{u-\alpha} = \frac{-\beta + u^2f(0) + u\left[\frac{df(x)}{dx}\right]_{x=0}}{(u-\alpha)u} \tag{A.22}$$

Afterwards, u is set to $-\alpha$:

$$A(s) = \frac{-\beta + \alpha^2f(0) - \alpha\left[\frac{df(x)}{dx}\right]_{x=0}}{2\alpha^2} \tag{A.23}$$

Using the defition in Equation A.8, this equation changes to:

$$\begin{aligned} A(s) &= \frac{-\beta + \alpha^2 \bar{C}_{red}(0,s) - \alpha \left[\frac{\delta \bar{C}_{red}(x,s)}{\delta x}\right]_{x=0}}{2\alpha^2} \\ &= \frac{-\beta}{2\alpha^2} + \frac{\alpha^2 \bar{C}_{red}(0,s)}{2\alpha^2} - \frac{\alpha \left[\frac{\delta \bar{C}_{red}(x,s)}{\delta x}\right]_{x=0}}{2\alpha^2} \\ &= \frac{-\beta}{2\alpha^2} + \frac{1}{2}\bar{C}_{red}(0,s) - \frac{1}{2\alpha}\left[\frac{\delta \bar{C}_{red}(x,s)}{\delta x}\right]_{x=0} \end{aligned} \tag{A.24}$$

$\bar{C}_{red}(0,s)$ can be found by setting $x = 0$ in Equation A.20 (remember, $B(s)$ has to be zero to comply to the boundary condition in Equation A.21):

$$\bar{C}_{red}(0,s) = \frac{\beta}{\alpha^2} + A(s)e^{-\alpha 0} + 0 \cdot e^{\alpha 0} = \frac{\beta}{\alpha^2} + A(s) \tag{A.25}$$

The Laplace transform of Equation A.4 yields:

$$D_{red}\left[\frac{\delta \bar{C}_{red}(x,s)}{\delta x}\right]_{x=0} = \frac{\bar{i}(s)}{nFA} \tag{A.26}$$

Combining Equations A.24, A.25 and A.26 results in:

$$A(s) = \frac{-\beta}{2\alpha^2} + \frac{1}{2}\left(\frac{\beta}{\alpha^2} + A(s)\right) - \frac{1}{2\alpha}\frac{\bar{i}(s)}{nFAD_{red}} \tag{A.27}$$

$$2A(s) = \frac{-\beta}{\alpha^2} + \frac{\beta}{\alpha^2} + A(s) - \frac{\bar{i}(s)}{\alpha nFAD_{red}} \tag{A.28}$$

$$A(s) = \frac{-\bar{i}(s)}{\alpha nFAD_{red}} \tag{A.29}$$

Filling in $A(s)$, $B(s)$ and $\Gamma(s)$ in Equation A.20 results in:

$$\bar{C}_{red}(x,s) = \frac{\beta}{\alpha^2} - \frac{\bar{i}(s)}{\alpha nFAD_{red}}e^{-\alpha x} \tag{A.30}$$

Using the defitions in Equation A.9 and Equation A.10, the following expression for $\bar{C}_{red}(x,s)$ is found:

$$\begin{aligned} \bar{C}_{red}(x,s) &= \frac{\frac{C^*_{red}}{D_{red}}}{\frac{s}{D_{red}}} - \frac{\bar{i}(s)}{nFA\sqrt{D_{red}s}}e^{-\sqrt{\frac{s}{D_{red}}}x} \\ &= \frac{C^*_{red}}{s} - \frac{\bar{i}(s)}{\sqrt{\frac{s}{D_{red}}}nFAD_{red}}e^{-\sqrt{\frac{s}{D_{red}}}x} \end{aligned} \tag{A.31}$$

B MATLAB simulation

In order to do the digital simulation of the diffusion profile as presented in Subsection 2.2.1, a MATLAB script was written. Listing B.1 shows this script. Running the simulation results in a number of MAT-files, a file format used by MATLAB to store variables, in order to save a concentration profile at a specific time step. To combine these files and plot the concentration level at a certain position at various times, a second MATLAB script can be found in Listing B.2.

Listing B.1: MATLAB script for the simulation of concentration profile as a result of diffusion

```
%% Script to calculate the concentration profile as a result of diffusion
 % for different times.
clear;
%% System constants
J = 15; % Current density [A/m^2]
D = 2E-9;   % Diffusion constant [m^2/s]
n = 1;  % Number of electrons taking part in the reaction per molecule []
F = 96485.3365; % Faraday's constant [s A/mol]
Cbulk = 10; % Bulk concentration [mol/m^3]

tau =((n*F*Cbulk/(2*J))^2*D*pi);     % Transition time (Sand equation)

% Simulation paramters
deltaT=1E-8;     % Time step [s]
deltaX=1E-8;     % Width of bin [m]
simTime=10;  % Time to be simulated [s]
numberOfBins=100000; % Number of bins in simulation
maxTime=floor(simTime/deltaT);  % Number of iterations needed

% Setup needed arrays
Cold=zeros(1,numberOfBins); % Concentration profile from previous iteration
Cnew=zeros(1,numberOfBins); % Concentration profile in current iteration

%% Calculate inital concentration profile from chronopotentiometry
position=0:deltaX:(numberOfBins-1)*deltaX;
for i=1:numberOfBins;
    Cold(i)=Cbulk-J/(n*F*D)*(2*sqrt(D*tau/pi)*exp(-(position(i))^2 ...
        /(4*D*tau))-(position(i))*erfc((position(i))/(2*sqrt(D*tau))));
end

%% Every _stepSize_ iteration, the concentration profile is stored in a file
stepSize=100000;

% Loop for iteration
for l=1:maxTime/stepSize
    for k = 1:stepSize
        Cnew(1)=0;  % Concentration in first bin is always zero
                    % (amperometry)
        Cnew(2:(numberOfBins-1))=Cold(2:(numberOfBins-1)) ...
```

```
            +D*deltaT/deltaX^2*(Cold(3:numberOfBins) ...
            -2*Cold(2:(numberOfBins-1))+Cold(1:(numberOfBins-2)));
            % New concentration profile is calculated from old profile
            % p787 in book by Bard et al.
        Cnew(numberOfBins)=Cbulk;   % Concentration far awar from electrode
                                    %is constant (bulk) concentration
        Cold(:)=Cnew(:);    % Old concentration profile is updated to new
                            %situation
    end
% Safe concetration profile in file after _stepSize_ iterations
    save(strcat('results\',int2str(l),'.mat'),'Cnew');
end

% fclose(fid);
```

Listing B.2: MATLAB script for importing the simulation results and plotting the data

```
  clear;
%% Script to calculate the concentration profile as a result of diffusion
% for different times.
clear;
% Simulation paramters
deltaT=1E-8;    % Time step [s]
deltaX=1E-8;    % Width of bin [m]
simTime=10;  % Time to be simulated [s]
numberOfBins=100000; % Number of bins in simulation
maxTime=floor(simTime/deltaT);  % Number of iterations needed
stepSize=100000; % Number of iterations in between MAT files
numberOfFiles=maxTime/stepSize;             % Number of MAT files resulting
                                            % from simulation

interestingX=5E-6;                          % x value that will be plotted
interestingIndex=floor(interestingX/deltaX+1); % Find simulation bin
                                               % nearest to asked x value
plotData=zeros(numberOfFiles,2);

for i=1:numberOfFiles
    load(strcat('results/',int2str(i),'.mat')); % load MAT file
    plotData(i,2)=Cnew(interestingIndex);   % Extract concentration of
                                            % specified bin
    plotData(i,1)=deltaT*stepSize*i;        % Calculate corresponding time
                                            % value
end;
%% System constants
J = 15; % Current density [A/m^2]
D = 2E-9;   % Diffusion constant [m^2/s]
n = 1;  % Number of electrons taking part in the reaction per molecule []
F = 96485.3365; % Faraday's constant [s A/mol]
Cbulk = 10; % Bulk concentration [mol/m^3]
E0=.22233;  % Standard potential Ag + Cl- <-> AgCl + e- [V]
R=8.314;    % Gas constant [J/(K mol)]
T=273;      % Absolute temperature [K]

tau =((n*F*Cbulk/(2*J))^2*D*pi);    % Transition time (Sand equation)
n=numberOfFiles;
%% Calculate Nernst potential based on simulation result
E=zeros(n+1,1);
xValues=zeros(n+1,1);
xValues(1)=tau;
for i=2:n+1
```

```
  E(i) = .22233+8.314*273*log(1/plotData(i-1,2))/F; % Calculate potential
  xValues(i) = tau+stepSize*deltaT*(i-1);   % Calculate corresponding time
                                            % value, add tau
end
%% Calculate concentration profile before tau
c = zeros(100,2);
x=interestingX;
for I=1:100;
    t=I/100*tau;
    C(I,2)=Cbulk-J*(2*(D*t/pi)^(1/2)*exp(-x^2/(4*D*t))...
        -x*erfc(x/(2*(D*t)^(1/2))))/(F*D); % Concentration profile from Bard
    C(I,1)=t;
end

%% Plot results
M(:,1)=C(:,1);
M(:,2)=E0+R*T/F*log(1./C(:,2));          % Calculate potential before tau
E(1)=M(end,2);                           % Graph should be (semi) continuous
figure(1);
plot(xValues/tau,E(:),M(:,1)/tau,M(:,2));   % Plot potential curve
line([1 1],[min([E(:)' M(:,2)']) max([E(:)' M(:,2)'])],'color','g','linestyle',':');
xlabel('time/\tau [s]');
ylabel('potential');

figure(2);
plot(xValues/tau,vertcat(C(end,2),plotData(:,2))/Cbulk,C(:,1)/tau...
    ,C(:,2)/Cbulk);          % Plot concentration curve
line([1 1],[0 1],'color','g','linestyle',':');
xlabel('time/\tau');
ylabel('normalized concentration');
```

C | Mask design

Each of the four designs is placed three times on the wafer, resulting in a total of 12 chips. Each chip is 15 by 20 mm and can be easily fitted in an available chip holder.

Two masks are needed during the fabrication process, one for defining the layers of the electrode and one to define where the polymer will cover the contact wires. Figure C.1 shows the full mask design. The black objects will form the metal electrodes, contact wires and contact pads. The part covered by the polymer is colored blue.

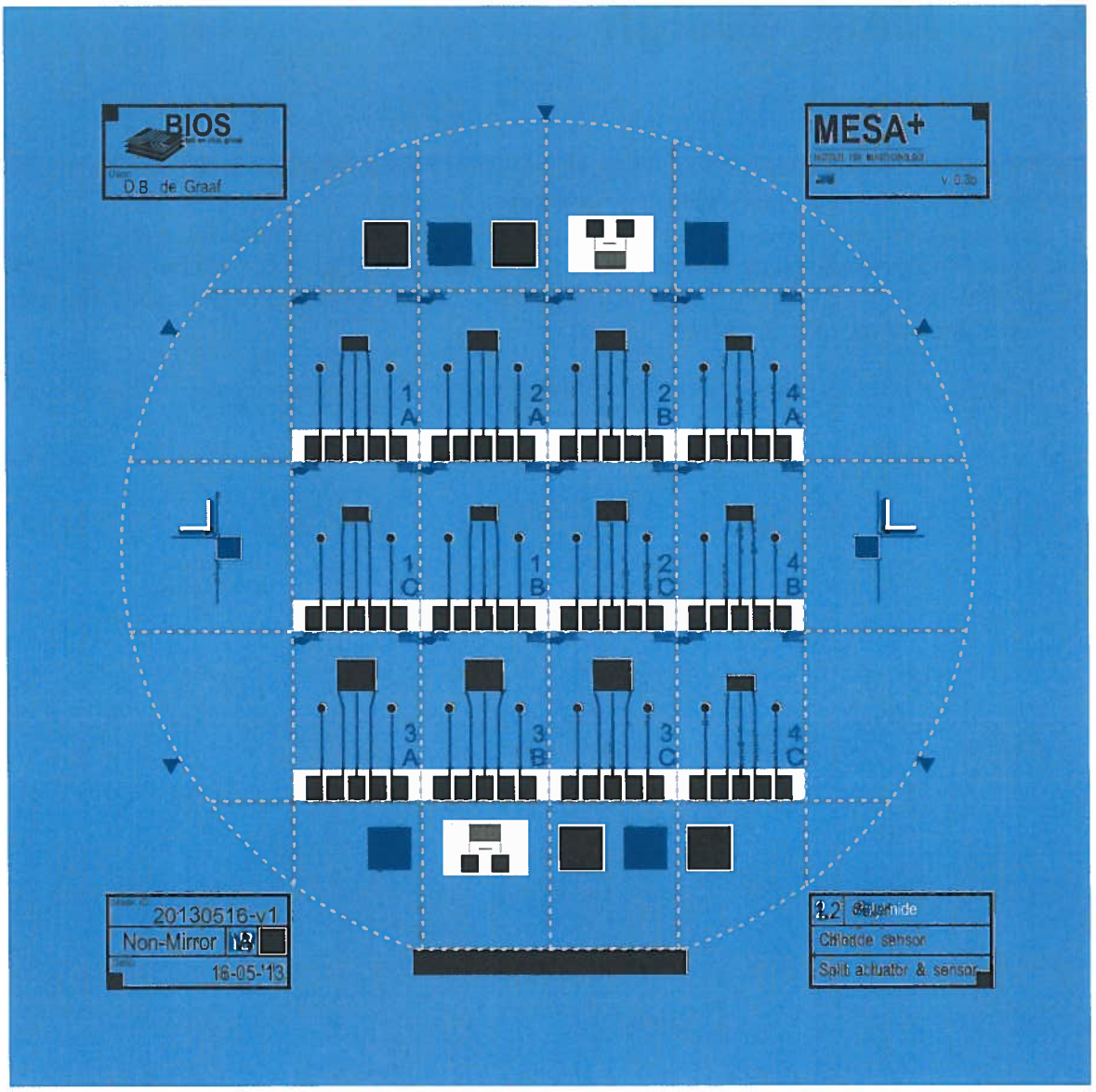

Figure C.1: Mask design for potentiometric devices with seperated sensor and actuator electrodes. Black structures will form the silver electrodes, contact wires and contact pads, blue colored parts will be covered by a polymer. Overlapping areas (dark blue) show silver structures covered by the polymer. The gray dotted line shows the wafer and chip outlines.

D | Chip fabrication

To convert the chip design of Chapter 3 into a physical chip, microfabrication is needed. The full cleanroom process is documented in the process document by Ing. Johan Bomer, which can be found on the next pages.

Process	: Ag electr. in glass and PI-passiv.	Revision	: 01	Pages	: 4
Project	: Chloride sensor for concrete	Rev. by	: J. Bomer	Created	: 08/13/133:59 PM
Author	: J. Bomer	File	: Glasswafer with buried...	Revised	: 08/13/133 59 PM

Glasswafer with buried Ag elektrodes and polyimide passivation

Material:
Borofloat wafers: 100 mm diameter and 500 µm thickness.
Determine the fronside by holding the wafer with the big flat towards yourself; if the small flat is on the left, than the upper side is the frontside.

Process sequence (schematic):

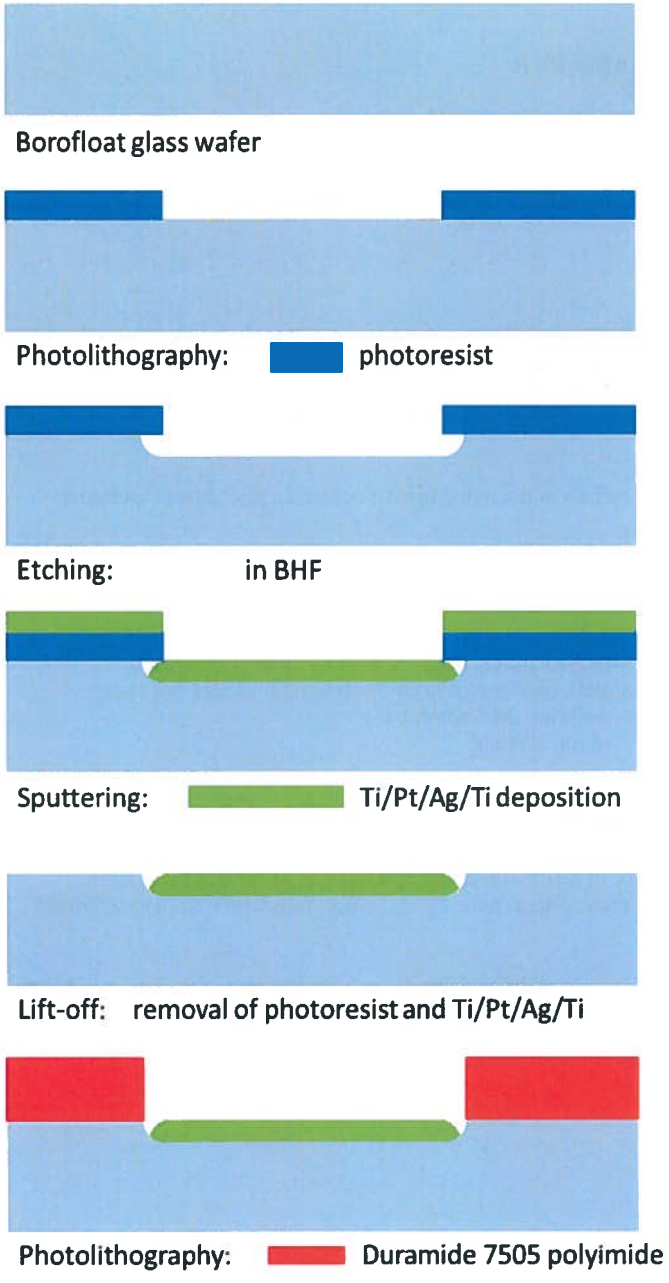

Process steps:

Cleaning:
- 2 min fuming HNO_3 I; wetbench 16
- QuickDumpRinse, QDR
- 10 sec 25 % KOH @ 75 °C dip; wetbench 17
- 10 min ultrasonic in the first rinse water; wetbench 16
- QDR
- 1 min fuming HNO_3 I + 2 min fuming HNO_3 II; wetbench 16
- QDR

Fotolithography:
purpose: applying etchmask and lift-off mask of fotoresist to define electrodes. Vapour fase HMDS is necessary to reduce undercutting!
- vapourfase fase (!) HMDS (see note 1)
- standard 17-resist process with 5,0 sec hard-contact exposure (see note 2)

Descum:
purpose: removal of residues of the lithography process; do, just prior to sputtering
- 5 min 120 °C
- 5 min UV ozon

Etching:
puropose: create a recces in glass
etchant: buffered HF (BHF metalfree) @ 19 °C (=temp. in de flowbench)
take your own BHF and leave it in the wetbench for at least one hour
time: 16 min 20 sec (etchrate: 24.5 nm/min)
goal: 400 nm result: 395 nm

Measuring:
purpose: check the etched depth
equipment: Dektak
prepare: scratch a piece of resist with a surgery knife e.g. at the alignment mark
measure: span: 1 mm, force: 5 mgr, time: 20 sec, mode: hills&valleys, range 6500 nm

Preconditioning:
purpose: removal of organic residues of storage and conditioning of the surface; do this just prior to sputtering
- 2 min 95 °C resist dehydration
- 5 min UV ozon

Sputtering:
purpose: deposition of the silver (Ag) electrodes; a titanium (Ti) layer is used to improve the adhesion, the platinum (Pt) layer should prevent interdiffusion of Ti and Ag and the final Ti layer should improve the adhesion of a passivating layer to the silver
DC-sputtergunsysteem "Sputterke"
backpressure <1E-6 mbar
parameters: Ar-sputterpressure: 5E-3 mbar (@ 110 sccm Ar);
DC-power: 200 W
sputter rate: Ti: 13 nm/min Pt: 25 nm/min Ag: 55 nm/min @200W
time: 1 min 30 sec Ti @ 180W
1 min 30 sec Pt @ 200W
5 min 30 sec Ag @ 200W
1 min 30 sec Ti @ 180W
result: nm Ti/Pt/Ag/Ti

remark 1: de uniformity after sputtering is about 10%; at the centre of the wafer the layer is thickest. Preferably, try to get the centre at level, than at the edge the platinum will be just under the glass surface. This prevents lift off problems.

Lift off:
purpose: removal of the photoresist with the sputtered metals on top
- 1 min ultrasonic in acetone (low grade)
- soak in acetone (low grade) until the metal is completely delaminated; it might take a few hours
- keep wafer wet with acetone and do 5 min ultrasonic in new acetone (low grade)
- rinse with acetone (high grade); keep wafer wet with acetone in between!
- rinse with IPA (high grade)
- spin dry

Measuring:
purpose: check whether the Platinum and glass surface is leveled
equipment: Dektak
- measure: span: 1 mm, force: 5 mgr, time: 20 sec, mode: hills&valleys, range 6500 nm
- wafer centre: 5 nm Pt below; wafer edge: 19 nm Pt below
- remark 2: the square resistance of the TaPt layer will be □ Ω.

Polyimide lithography:
purpose: apply a passivating layer and pattern it (by photolithography) to open the active area of the silver and the contactpads
- 5 min UV ozon
  (after this the Ti looks a little yellowish, because of oxidation of the Ti surface)
- 5 min 120 °C wafer dry step
- spin: 30 sec 3500 rpm Durimide 7505
- 5 min 100 °C polyimide dry step
- exposure: 4 sec, with hard contact mode at least 1 bar
- relaxation: leave for 1 hour at room temperature
- development in HTR-D2: 20 sec beaker I, 20 sec beaker II (shaked constantly, 5 sec ultrasonic, rinse with RER600, rinse with IPA, spindry
- cure: 105 min at 350 °C in 2 mbar N_2 , vacuum furnace (45 min ramp up is included)

RIBE:
purpose: removal of Ti (and Pt) from the active area and contact pads
equipment: ReactiveIonBeam Etcher, Oxford i300
- beam: 300V 50 mA. angle: -20 °
- time: 6 min for Ti and 5 min for Pt
- 5 min UV ozon

Dicing:
purpose: cut the wafer in chips
equipment: Loadpoint dicing machine
- use the blue dicing foil (70 µm thick)
- laminate the wafer onto the blue dicing foil in frame and leave for 5 min on the 70 °C hotplate
- use the TC300 blade (300 µm thick) at speed 4.0 mm/sec, total thickness 570 µm, cut depth: 510 µm

note 1:
Vapour phase HMDS
equipment: HMDS, home made setup in wetbench 28
- put the wafers in the oven, close the door and leave it for 5 min at atmospheric pressure to heat up the wafers
- open the vacuum valve to pump down
- open the N_2 valve to purge until pressure is -100 Torr, then close it
- repeat previous step
- wait until pressure is - Torr
- open the HMDS valve
- close the vacuum valve
- wait for 10 min
- open the vacuum valve
- open the N_2 valve to purge until pressure is -100 Torr, then close it
- wait until pressure is - Torr
- close the vacuum valve
- open the N_2 valve to ventilate system
- unload your wafers
- pump down the system by opening the vacuum valve

note 2:
Fotolithography Olin17:
equipment: positive resist 1, wetbench 21
material: Olin 908/17 positive photoresist

- spin parameters: prog. 7: (10 sec 500 rpm @ 500 rpm/sec
  + 30 sec 4000 rpm @ 500 rpm/sec)
- dry: 2 min @ 95 ^{o}C
- exposure: 5 sec, with hard contact mode at least 1 bar
- development: 30 sec beaker I (OPD4262)
  15 sec beaker II (OPD4262)
- QDR
- spindry
- hardbake: 30 min 120 ^{o}C

E | Data analysis scripts

To analyze the many data files that result from the experiments as presented in Chapter 4, a number of MATLAB scripts have been written to import the data from the BioLogic EC-Lab software, detect the transition point and export this transition data for plotting.

As the format of the exported MPT-files differ, depending on the type of experiment that was run, two MATLAB import functions were written. Listing E.1 shows the import of files that result from the chronopotentiometric of the first channel (refer to Subsection 4.4.2). Listing E.2 shows the import of files from OCV experiments, as are run on the second channel of the potentiostat.

Listing E.1: MATLAB script to import MPT files of chronopotentiometric experiments from EC-lab

```
function data=readEClab(fileName)
%data = readEClab(fileName)
%   Imports data from EC-Lab MPT files. Written to import files that are
%   the result of chronopotentiometry. MPT files from other types of
%   experiments probably need adaptations in this function.
%   fileName:   string containing file to import
%
%   Author: Derk de Graaf

% open the file, exit function if file does not exist
fid=fopen(fileName);
if fid<0
    data=[];
    return;
end

% ignore first line
fgets(fid);

% read line and extract number of header lines.
headerInfo=fgets(fid);
headerLine=textscan(headerInfo,'%*s%*s%*s%*s%u');

% read file again and convert commas to dots
fileData=strrep(fileread(fileName),',','.');

% extract two colums with data out of the file, ignoring the header lines
data=textscan(fileData, ...
    '%*f␣%*f␣%*f␣%*f␣%*f␣%*f␣%f␣%*f␣%f␣%*f␣%*f␣%*f␣%*f', ...
    'headerlines',headerLine{1});

% close the file
fclose(fid);
end
```

Listing E.2: MATLAB script to import MPT files of OCV experiments from EC-lab

```
function data=readEClabOCV(fileName)
%data = readEClabOCV(fileName)
%   Imports data from EC-Lab MPT files. Written to import files that are
%   the result of open cell voltage (OCV) measurements. MPT files from
%   other types of experiments probably need adaptations in this function.
%   fileName:   string containing file to import
%
%   Author: Derk de Graaf

% open the file, exit function if file does not exist
fid=fopen(fileName);
if fid<0
    data=[];
    return;
end

% ignore first line
fgets(fid);

% read line and extract number of header lines.
headerInfo=fgets(fid);
headerLine=textscan(headerInfo,'%*s%*s%*s%*s%u');

% read file again and convert commas to dots
fileData=strrep(fileread(fileName),',','.');

% extract two colums with data out of the file, ignoring the header lines
data=textscan(fileData,'%*f␣%*f␣%f␣%f','headerlines',headerLine{1});

% close the file
fclose(fid);
end
```

To automate the analysis of a number of files, two scripts are written which process a series of files, in which one (numeric) value in the file name changes, e.g. a chloride concentration level indicated in the file name. The functions are made specific for either a sensor (Listing E.3) or actuator (Listing E.4), using the previously mentioned import functions.

Listing E.3: MATLAB script to analyze multiple MPT files of sensor measurements from EC-lab

```
function [output]=dataAnalysisChipsSensor(values,fileName1,fileName2,offset)
%output = dataAnalysisChipsSensor( values , fileName1 , fileName2 , offset )
%   Function to analyze a series of measurement files. Function can only
%   analyze OCV measurements.
%   ouput:  array of determining value and corresponding transition time
%   values: array of determining values (numbers identifying each of the
%           measurement files)
%   fileName1:  string containing first part of the file name
%   fileName2:  string containing second part of the file name
%   offset: time at which the current pulse was started [s]
%
%   Author: Derk de Graaf

data=zeros(numel(values),2);

% start for-loop to analyze all requested files
for i=1:numel(values)
    % combine both file name strings to one using the array of identifying
    % numbers and import the corresponding MPT file.
    fileName=(strcat(fileName1,num2str(values(i)),fileName2));
```

```
    F=readEClabOCV(fileName);

    % if the file exists, continue to find the transition time, otherwise
    % return an empty array
    if isempty(F)==false
        transition=findTransitionChips([F{1,1} F{1,2}], ...
            strcat(num2str(values(i)),'mM_KCl'),offset);
    else
        transition=[];
    end

    % if transitions are found, copy them to the output.
    if isempty(transition)==false
        data(i,2)=transition;
        data(i,1)=values(i);
    end
end

% if no transitions are found, return an empty array
data( ~any(data,2), : ) = [];
output=data;
end
```

Listing E.4: MATLAB script to analyze multiple MPT files of actuator measurements from EC-lab

```
function [output]=dataAnalysisChipsActuator(values,fileName1,fileName2,offset)
%output = dataAnalysisChipsActuator( values , fileName1 , fileName2 , offset )
%   Function to analyze a series of measurement files.
%   ouput: array of determining value and corresponding transition time
%   values: array of determining values (numbers identifying each of the
%           measurement files)
%   fileName1: string containing first part of the file name
%   fileName2: string containing second part of the file name
%   offset: time at which the current pulse was started [s]
%
%   Author: Derk de Graaf


data=zeros(numel(values),2);

% start for-loop to analyze all requested files
for i=1:numel(values)
    % combine both file name strings to one using the array of identifying
    % numbers and import the corresponding MPT file.
    fileName=(strcat(fileName1,num2str(values(i)),fileName2));
    F=readEClab(fileName);

    % if the file exists, continue to find the transition time, otherwise
    % return an empty array
    if isempty(F)==false
        transition=findTransitionChips([F{1,1} F{1,2}], ...
            strcat(num2str(values(i)),'mM_KCl'),offset);
    else
        transition=[];
    end

    % if transitions are found, copy them to the output.
    if isempty(transition)==false
        data(i,2)=transition;
        data(i,1)=values(i);
```

```
    end
end

% if no transitions are found, return an empty array
data( ~any(data,2), : ) = [];
output=data;
end
```

The actual determination of the transition time is done in the script of Listing E.5. This script takes the first derivative of (a filtered version of) the measured potential, finds the location of the maximum value of this derivative and returns the corresponding time value.

Listing E.5: MATLAB script for the detection of the biggest inflection point in a dataset

```
function [ transitionPoint ] = findTransitionChips(data,titleData,offset)
%transitionPoint = findTransitionChips( data , titleData , offset )
%   Detection of the inflection point.
%   transitionPoint:    Time of inflection point [s] Relative to offset
%   data:               Array with data points in form [time value]
%   titleData:          String with information about the data to put in
%                       plot
%   offset:             Time at which the current pulse was started [s]

% find first data point after the offset time. For better results, the
% actual starting point is taking a little after the offset time, since
% otherwise the start peak is mistakenly detected as the inflection point
startPoint=1;
while data(startPoint,1) < (offset+.1)
    startPoint = startPoint + 1;
end

% the part of the data to be observed ends at the highest value. A few
% datapoints are omitted at the end to prevent de abrupt stop at the end to
% be detected as inflection point.
[~, maxLocation]=max(data(:,2));
endPoint=maxLocation-5;

% smaller datasets are defined based on the above start and end point
dataSubset{1}=data(startPoint:endPoint,1);
dataSubset{2}=data(startPoint:endPoint,2);

% the data subset is filtered using a moving average filter. The derivative
% of the filtered data is then taken
dydt=smooth(diff(dataSubset{2}),75)./diff(dataSubset{1});
dt = diff(dataSubset{1}(1:end)) + dataSubset{1}(1:end-1);

% the highest peak of the derivative is determined
[peakFit,locsFit] = findpeaks(dydt);
[~, maxIndex] = max(peakFit);
peakLocation=locsFit(maxIndex);

% in case no peak is detected, an error message is presented along with a
% plot of the data and derivative of the data. Then the function ends
% returning an empty array.
if isempty(peakLocation)
    msgbox(strcat({'No␣peak␣detected␣at␣'},titleData,'!'), ...
        'Peak␣detection␣error','error');
    figure;
    plot(dt,dydt,'r');
    hold on;
```

```
    plot(data(:,1),data(:,2),'b');
    xlabel('time [s]');
    ylabel('potential [V]');
    title(strcat({'Polynomial fit on measurement data for: '},titleData));
    hold off;
    transitionPoint=[];
    return;
end

% the time at which the inflection point is detected is calculated
transitionPoint=dt(peakLocation)-offset;

% a plot of the data and derivative of the data is presented and the
% function ends normally.
figure;
hold on;
plot(data(:,1),data(:,2),'b');
plot(dt,dydt,'r');
line([dt(peakLocation) dt(peakLocation)],[0 max(dataSubset{2})], ...
    'color','k','linestyle',':');
text(dt(peakLocation), .2, num2str(dt(peakLocation)-offset));
xlabel('time [s]');
ylabel('potential [V]');
title(strcat({'Polynomial fit on measurement data for: '},titleData));
hold off;
end
```